NAVAL POSTGRADUATE SCHOOL
Monterey, California

THESIS

DESIGN OF A MINI THERMO-ACOUSTIC REFRIGERATOR

by

Seyhmus Direk

March 2001

Thesis Advisor:	Thomas J. Hofler
Second Reader:	Richard Harkins

20010614 116

REPORT DOCUMENTATION PAGE		Form Approved OMB No. 0704-0188

Public reporting burden for this collection of information is estimated to average 1 hour per response, including the time for reviewing instruction, searching existing data sources, gathering and maintaining the data needed, and completing and reviewing the collection of information. Send comments regarding this burden estimate or any other aspect of this collection of information, including suggestions for reducing this burden, to Washington headquarters Services, Directorate for Information Operations and Reports, 1215 Jefferson Davis Highway, Suite 1204, Arlington, VA 22202-4302, and to the Office of Management and Budget, Paperwork Reduction Project (0704-0188) Washington DC 20503.

1. AGENCY USE ONLY *(Leave blank)*	2. REPORT DATE March 2001	3. REPORT TYPE AND DATES COVERED Master's Thesis	
4. TITLE AND SUBTITLE Design Of A Mini Thermo-Acoustic Refrigerator		5. FUNDING NUMBERS	
6. AUTHOR(S) Seyhmus Direk			
7. PERFORMING ORGANIZATION NAME(S) AND ADDRESS(ES) Naval Postgraduate School Monterey, CA 93943-5000		8. PERFORMING ORGANIZATION REPORT NUMBER	
9. SPONSORING / MONITORING AGENCY NAME(S) AND ADDRESS(ES)		10. SPONSORING / MONITORING AGENCY REPORT NUMBER	

11. SUPPLEMENTARY NOTES

The views expressed in this thesis are those of the author and do not reflect the official policy or position of the Department of Defense or the U.S. Government.

12a. DISTRIBUTION / AVAILABILITY STATEMENT Approved for public release; distribution is unlimited.	12b. DISTRIBUTION CODE

13. ABSTRACT *(maximum 200 words)*

     A miniature thermoacoustic refrigerator is being developed for the purpose of cooling integrated circuits below their failure temperature when used in hot environments. The development of an electrically powered acoustic driver that powers the thermoacoustic refrigerator is described. The driver utilizes a flexural tri-laminar piezoelectric disk to generate one to two Watts of acoustic power at 4 kHz in 15 bar of He-Kr gas mixture. This thesis is the second of two driver development theses, which includes the information on the assembly of three drivers and their quantitative performance with a pressurized test resonator. A maximum acoustic power output of 0.5 Watt was achieved with the third driver.

14. SUBJECT TERMS thermoacoustic refrigerator, TAR, thermo-acoustic refrigerator driver, microchip cooling	15. NUMBER OF PAGES 106
	16. PRICE CODE

17. SECURITY CLASSIFICATION OF REPORT Unclassified	18. SECURITY CLASSIFICATION OF THIS PAGE Unclassified	19. SECURITY CLASSIFI- CATION OF ABSTRACT Unclassified	20. LIMITATION OF ABSTRACT UL

NSN 7540-01-280-5500

Standard Form 298 (Rev. 2-89)
Prescribed by ANSI Std. 239-18

THIS PAGE INTENTIONALLY LEFT BLANK

DESIGN OF A MINI THERMO-ACOUSTIC REFRIGERATOR

Seyhmus Direk
Lieutenant Junior Grade, Turkish Navy
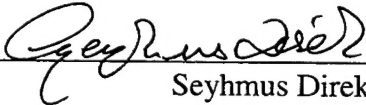B.A., Turkish Naval Academy, 1995

Submitted in partial fulfillment of the
requirements for the degree of
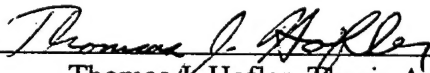
MASTER OF SCIENCE IN ENGINEERING ACOUSTICS

from the
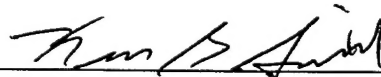
NAVAL POSTGRADUATE SCHOOL
March 2001

Author: _____
Seyhmus Direk

Approved by: _____
Thomas J. Hofler, Thesis Advisor

_____
Richard Harkins, Second Reader

_____
Kevin Smith, Chairman
Engineering Acoustics Academic Committee

iii

THIS PAGE INTENTIONALLY LEFT BLANK

ABSTRACT

A miniature thermoacoustic refrigerator is being developed for the purpose of cooling integrated circuits below their failure temperature when used in hot environments. The development of an electrically powered acoustic driver that powers the thermoacoustic refrigerator is described. The driver utilizes a flexural tri-laminar piezoelectric disk to generate one to two Watts of acoustic power at 4 kHz in 15 bar of He-Kr gas mixture. This thesis is the second of two driver development theses, which includes the information on the assembly of three drivers and their quantitative performance with a pressurized test resonator. A maximum acoustic power output of 0.5 Watt was achieved with the third driver.

THIS PAGE INTENTIONALLY LEFT BLANK

TABLE OF CONTENTS

LIST OF FIGURES

LIST OF TABLES

THIS PAGE INTENTIONALLY LEFT BLANK

ACKNOWLEDGMENTS

I would like to thank Professor Hofler and Professor Harkins for their instruction, assistance, and patient guidance during this thesis project. Thanks also to Jayy Adeff for all his assistance. Special thanks to my parents and my family for supporting me whole my life.

THIS PAGE INTENTIONALLY LEFT BLANK

I. INTRODUCTION

Thermoacoustic refrigeration uses advanced acoustic technology to improve cooling capacity without the need for environmentally destructive refrigerants. The subject of Dr. Thomas Hofler's doctoral research, the thermoacoustic refrigerator is a testbed for thermoacoustic theory and a major step toward achieving a practical thermoacoustic cryocooler.

The mechanism of the thermoacoustic refrigerator (TAR) is simple, and is based on the expansion and compression of a gas in the form of a sound wave. When a sound wave from a vibrating diaphragm or a loudspeaker is sent down a hollow, half-wavelength tube, the pressure pulsations cause oscillatory motion of the gas in the axial direction in the form of a standing wave.

The combination of the pressure oscillations and oscillatory motion of the gas causes heat transport where the gas is in thermal contact with a stationary surface. When a small structure with a large amount of surface area is placed in the sound wave, at the appropriate location, substantial amounts of heat transport will occur. This structure is usually called a "stack"; one end is cooled by the heat transport and the other end heated. If the ends of the stack make thermal contact with heat exchangers, a functional heat pump or refrigerator can be constructed.

A. OBJECTIVE

The goal of this thesis project is to design and build a miniature thermoacoustic refrigerator (TAR) for micro-electronic integrated circuit cooling. It uses a custom piezoelectric driver and a copper and stainless steel tube resonator. This mini TAR is intended to match the current levels of efficiency and durability of existing thermoelectric (TE) coolers and possible surpass TE coolers with subsequent revisions. TAR technology is also free of the modest upper temperature limitations inherent in current generation high-efficiency TE cooling technology. Such TE coolers are limited to a sustained hot temperature of only 85 C.

B. THESIS ORGANIZATION

Chapter II provides a basic foundation for the development and current applications of TARs and piezoelectric devices. This chapter gives information about thermoacoustic principles.

Chapter III explains in detail the assembly of the mini TAR.

Chapter IV shows the design of the copper test resonator, and briefly discusses how this resonator was built using Design Simulation Thermoacoustic Research (DSTAR).

Chapter V details the measurements of the piezoelectric driver with the test resonator. The test resonator has adjustable length and resonant frequency. These measurements allow the driver to be characterized in

the operable frequencies and amplitude or acoustic power delivered over those frequencies.

Chapter VI describes the construction of the second driver, which is tested with two piezoelectric disks. The chapter also presents the data gathered while using this driver.

Chapter VII presents test results of the second driver's performance after its piezoelectric disks and steel diaphragm had been changed. This chapter also provides measurements taken following the addition of lead mass to the piezoelectric disk.

Chapter VIII explains the basic criteria for designing the mini TAR, DSTAR models, its theoretical results as well as the basic hardware design of the refrigerator resonator.

In concluding the thesis, Chapter IX offers general observations and recommendations for the proposed mini TAR model, as well as suggestions for future research and development.

THIS PAGE INTENTIONALLY LEFT BLANK

II. BACKGROUND

A.   THERMOACOUSTIC HEAT ENGINES

Thermoacoustic engines can be classified as heat pumps or prime movers (Fig. 2.1). In a heat pump, heat is transferred from an area with a low temperature to one with a high temperature, and during this transfer, the engine absorbs work. In a prime mover, heat flows through the engine from an area of higher temperature to one of a lower temperature, and the engine generates work as a result of this process. Fig. 2.1 shows that the processes of prime movers and heat pumps are the reverses of each other.

More specifically, a thermoacoustic heat pump uses a finite-amplitude standing acoustic wave to transport thermal energy incrementally along a thermoacoustic "stack" from one heat exchanger to another. The acoustically generated heat transfers, produces a significant thermal gradient over the length of the stack. This conversion of acoustic energy into stored thermal energy can be used for a wide variety of diverse applications, including refrigeration.

This process, followed in a reverse order, closely resembles the workings of a thermoacoustic prime mover, in which stored thermal energy from an external source is converted into kinetic energy in the form of acoustic waves. The conversion of energy occurs when heat delivered by a heat exchanger causes a temperature differential of sufficient magnitude over the length of a stack, causing acoustic instability in the internal gas. This

instability results in an initial exponential rise in amplitude with a growth rate that increases with the temperature gradient, and a frequency given by the natural resonance, (e.g., the resonance may be determined by a quarter wavelength tube resonance.) After the initial exponential growth, the amplitude will reach a limit determined by the complex nonlinear interplay between heat-exchanger conduction, acoustic dissipation and loading characteristics.

The primary attraction of thermoacoustic heat engines is that they can be constructed in a range of sizes, allowing for a large variety of applications. When compared to conventional heat engines, thermoacoustic engines are extremely simple and inherently reliable. They also feature another significant benefit in that they do not require chlorofluorocarbons (CFC's) or other environmentally damaging substances.

B.   THE THERMOACOUSTIC PROCESS

A complete analytical analysis of the thermoacoustic process is provided by Swift (Ref 1,3), and is used as the basis for the following description.

1.   Efficiency and The Carnot Cycle

Reversible heat engines will operate in one of two modes -- as a prime mover or as a heat pump. As a prime mover, the application of thermal energy from two reservoirs of different temperature will generate useful work within the engine. As a heat pump, the application
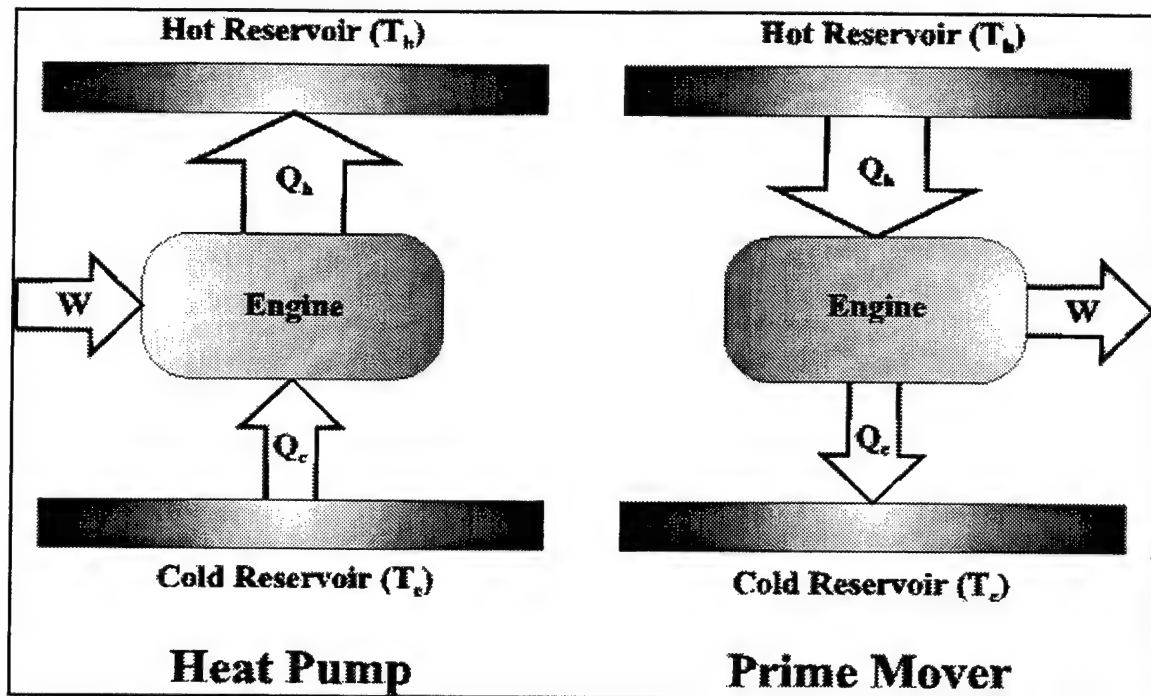
Figure 2.1. Heat Engine Operation (From: Livvarcin, 2000, pp. 9)

of work to the engine will cause heat energy to flow from a region of lower temperature to one of higher temperature

The First and Second Laws of Thermodynamics place a limit on the efficiency of any process involving the use of heat engines. This limit depends solely on the temperatures of the two reservoirs used by the heat engine. For expressing this fact in an equation let T_H and T_C be the temperature of the hot and cold reservoirs, Q_H and Q_C the associated heat flows, and W, the work flow as shown in Fig. 2.1. We assume a steady state operation. In the

7

usual case of cyclic operation, Q_H, Q_C and W are time-averaged powers, so that the time-averaged state of the engine does not change itself.

The First Law of Thermodynamics states that the energy of a system must be conserved:

$$Q_H - Q_C = W \tag{2.1}$$

The Second Law of Thermodynamics states that the total entropy, generated by any real process, must be positive or zero. Additionally, entropy is proportional to the heat flow to a reservoir divided by the temperature of that reservoir, therefore the 2nd Law can be expressed as:

$$\frac{Q_C}{T_C} - \frac{Q_H}{T_H} \geq 0 \text{ (Prime Mover)} \tag{2.2}$$

or

$$\frac{Q_H}{T_H} - \frac{Q_C}{T_C} \geq 0 \text{ (Heat Pump)} \tag{2.3}$$

In the case of a prime mover, the efficiency, (the ratio of desired output to the required input) can be defined as,

$$\eta = \frac{W}{Q_H} \tag{2.4}$$

By using equations (2.1) and (2.2), Q_H can be defined as a parameter of W, T_H and T_C,

$$Q_H - Q_C - W = 0 \Rightarrow Q_C = Q_H - W$$

$$\frac{Q_C}{T_C} - \frac{Q_H}{T_H} \geq 0 \Rightarrow \frac{Q_H(T_H - T_C)}{T_H T_C} \geq \frac{W}{T_C} \Rightarrow Q_H \geq \frac{W T_H}{[T_H - T_C]}$$

Combining this expression of Q_H into equation (2.4) we get,

$$\eta \leq \frac{T_H - T_C}{T_H} \qquad (2.5)$$

The temperature ratio on the right side of equation (2.5) called *Carnot efficiency*, represents the upper bound which any prime mover can achieve.

We also define a dimensionless quantity, *the coefficient of performance* (COP) which can be calculated for a perfect or Carnot engine.

In the case of an engine operating as a heat pump, efficiency is called the COP, and is given by:

$$COP = \frac{Q_C}{W} \qquad (2.6)$$

where Q_C is the desired effect for the engine, and the input power W is energy usage required by the engine to achieve this heat transfer operation. By combining equations (2.1), (2.3) and (2.6) and eliminating Q_H :

$$COP_C \leq \frac{T_C}{T_H - T_C} \qquad (2.7)$$

The right side of the inequality is an upper limit of the COP, and can be much greater than unity for a small temperature span refrigerator. In this

case, COP is used rather than "efficiency," because the latter refers to a quantity that has an upper limit of unity.

The Carnot Cycle, as shown in Fig. 2.2, represents the ideal thermodynamic cycle in which the net increase in entropy over the cycle is zero.

For this ideal cycle, there are two isothermal steps in which work and heat flow into or out of the engine, and two adiabatic steps in which compression and expansion of the fluid medium occurs. When carried out at near equilibrium conditions, the total increase in the entropy of the system during the expansion step is exactly equal to the total drop in the entropy during the compression step. Any real thermodynamic engine generating useful work will not operate under these conditions, and will therefore have a net increase in the total entropy over one cycle. It is for this reason that the Carnot Cycle represents the upper bound of the possible efficiency of any heat engine, be it a prime mover or a heat pump.

C.   THERMOACOUSTIC ENGINES

1. Engine Design

A thermoacoustic engine converts thermal energy from a high temperature heat source into useful work, in the form of acoustic power, while diverting waste thermal energy into a cold heat sink. To accomplish this task, several components are required. The first component is the hot

10
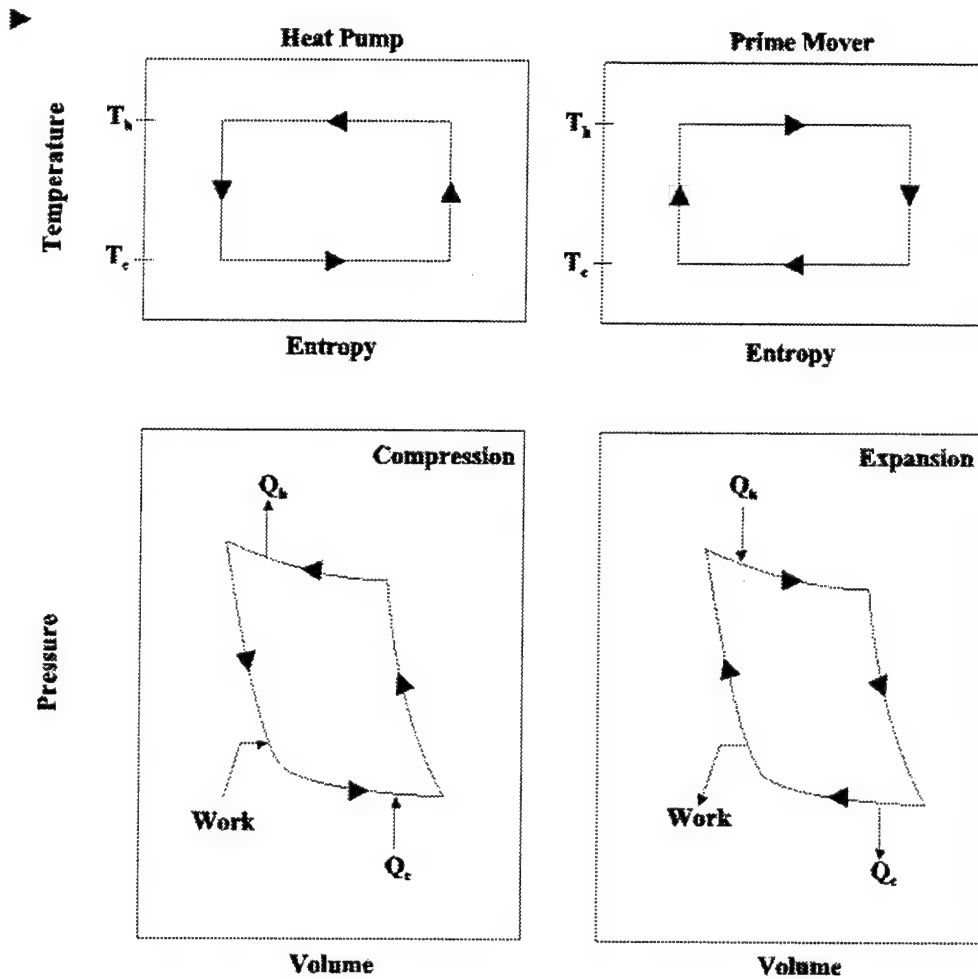
The Carnot Cycle

Figure 2.2. The Carnot Cycle temperature-entropy (T-S) and Pressure-Volume (P-V) diagrams for both the prime mover and heat pump. The near equilibrium state of the cycle ensures that the total change in entropy over one cycle is zero. This yields the rectangular plot in the T-S diagram, and ensures that the total work added to or removed from the engine is equal to the area enclosed by the P-V cycle. (From: Livvarcin, 2000, pp. 10)

heat exchanger. The first part of heat exchanger is a means for the high thermal energy to enter the engine, referred to as the hot heat exchanger. The second component is the cold heat exchanger, whose function is to expel waste thermal energy from the engine into the cooler heat sink.

The stack is one of the other critical components of the thermoacoustic engine, which is placed between the cold and the hot heat exchangers. It is a set of precisely spaced metal plates, or a multilayered (rolled) combination of polyester plastic film and monofilament line used as a buffer between layers. The purpose of the stack is to provide a means of temporary heat storage and a smooth temperature gradient from the hot heat exchanger to the cold heat exchanger.

Stack layers create channels through which the acoustic wave can travel. These layers lie parallel to the direction of the propagation wave, and serve as a conduit for the transfer of heat and acoustic power. Some acoustic power is dissipated in the stack because of the heat transportation process.

The final component is the resonator tube, which determines the operation of the engine. The resonator contains the thermoacoustic engine's stack and heat exchangers. As explained by Swift [Ref, 1,3], the resonator should have a high quality factor Q, to minimize the dissipation of acoustic power into heat. This tube determines the frequency of the acoustic energy produced by the engine.

A standing wave exists in the resonant tube. One end of the stack is placed very near a pressure antinode of the standing wave. The interaction between the oscillating gas in the channels of the stack, and the stack surfaces cause heat to be transported from one end of the stack to the other. The direction of the heat transport is towards the nearby pressure antinode.

The compression and expansion of the gas in the channel are neither adiabatic nor isothermal. Therefore, temperature oscillations of the gas exist, and heat also diffuses transversely between the gas and the adjacent solid surface area.

In a rigid-open end terminated tube configuration, as shown in Fig. 2.3, that the lowest resonant mode is a quarter wavelength with pressure anti-nodes at the closed end and pressure nodes at the open end. This configuration ensures that the fundamental mode will have a wavelength approximately four times the length of the tube.

Other configurations are possible, including a closed end resonator with pressure nodes at both ends producing acoustic power at a wavelength two times the physical length of the tube.

2. Thermoacoustic Requirements and the Thermodynamic Cycle

For the purposes of clarifying the operation of a thermoacoustic heat engine, this thesis will provide an explanation based on the Lagrangian

13

approach to define the thermoacoustic effect. A finite particle of gas is also followed to demonstrate the elements of the thermoacoustic effect.

Guided by the Lagrangian, we follow a given parcel of gas as it moves, Fig. 2.4. We can simplify by assuming that the oscillations are square-waves. The cycle consists of reversible adiabatic steps and two irreversible constant-pressure steps, which are identical to Brayton Cycle [Ref. 4].

Phasing is an important factor in a standard heat engine's operation. In a traditional heat engine, the crankshaft and camshaft are controlling the movement of pistons and valves mechanically. Pistons and valve must be coordinated so the working medium can be transported through the desired thermodynamic cycle.

In the thermoacoustic engine, there are no mechanical parts to perform these functions. The key to phasing in an acoustic engine is the presence of two thermodynamic media, the gas parcel and the plate.

As the gas parcel oscillates along the plate, its temperature is changed. This change in temperature is a result of adiabatic compression and expansion of the gas by the sound pressure, and from the plate's temperature.

The heat flow between the gas and the plate creates a necessary time delay or time phasing between temperature and pressure. The time delay arising from the irreversible heat transfer process is needed to ensure the operation of thermoacoustic engines. In other words, thermal conduction is

14
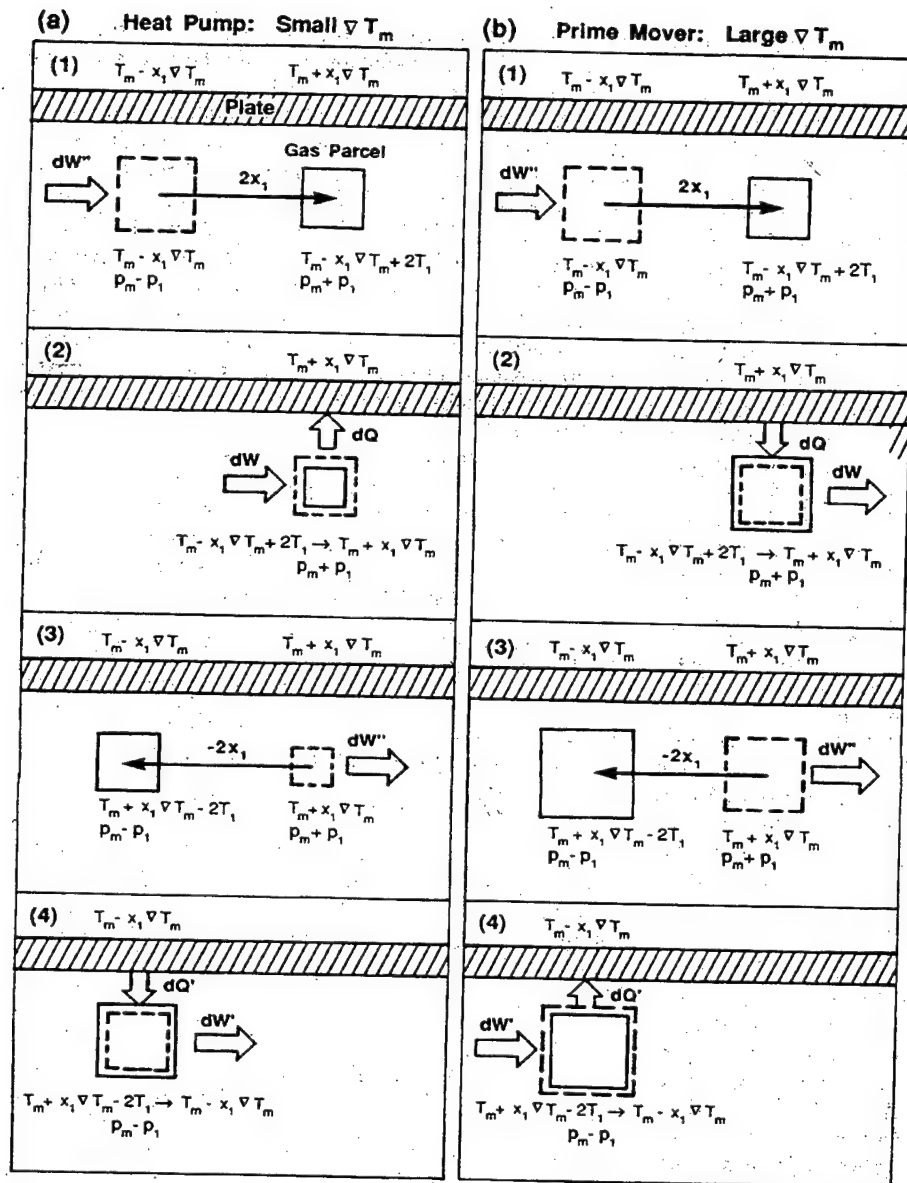
Figure 2.3 Typical fluid parcels in (a) a thermoacoustic heat pump and (b) a thermoacoustic prime mover, experiencing a four step cycle with two adiabats and two constant-pressure heat transfers (From: Swift, 1988, pp. 1155)

necessary to achieve the proper phasing of the temperature oscillations at the working gas parcel.

If the thermal conductivity is too high, the change in temperature of the gas parcel will occur too rapidly, and therefore no time delay will be created. If the thermal conductivity is too low, no appreciable temperature change will occur, and the cycle will not be driven.

The magnitude of the temperature gradient along the plate determines the sign of the phasing and the mode of the acoustic heat engine. The parcel of the gas is warmed and displaced during the compression of an acoustic standing wave. As a result, two temperatures are important to that parcel: the gas temperature after adiabatic compression and plate temperature next to the gas parcel after compression and displacement. If the gas temperature is lower than the plate's temperature, heat flows from plate to gas. If gas temperature is higher then that of the plate, heat will flow from gas to plate.

Altering the size of the temperature gradient will allow both, heat and work flows to be reversed, and the engine to operate as a prime mover or a heat pump. A high gradient is the condition for a prime mover, a zero or low gradient is the condition for a heat pump.

Figure 2.4 shows the movement, heat transfer, and volume changes of a parcel of gas as it moves during one cycle. Initially, the gas parcel is stationed at one thermal penetration depth from the plate in a region of a high acoustic pressure gradient. The high-pressure gradient drives the parcel

ACOUSTIC HEAT ENGINE CYCLE (HOFLER TUBE - PRIME MOVER)
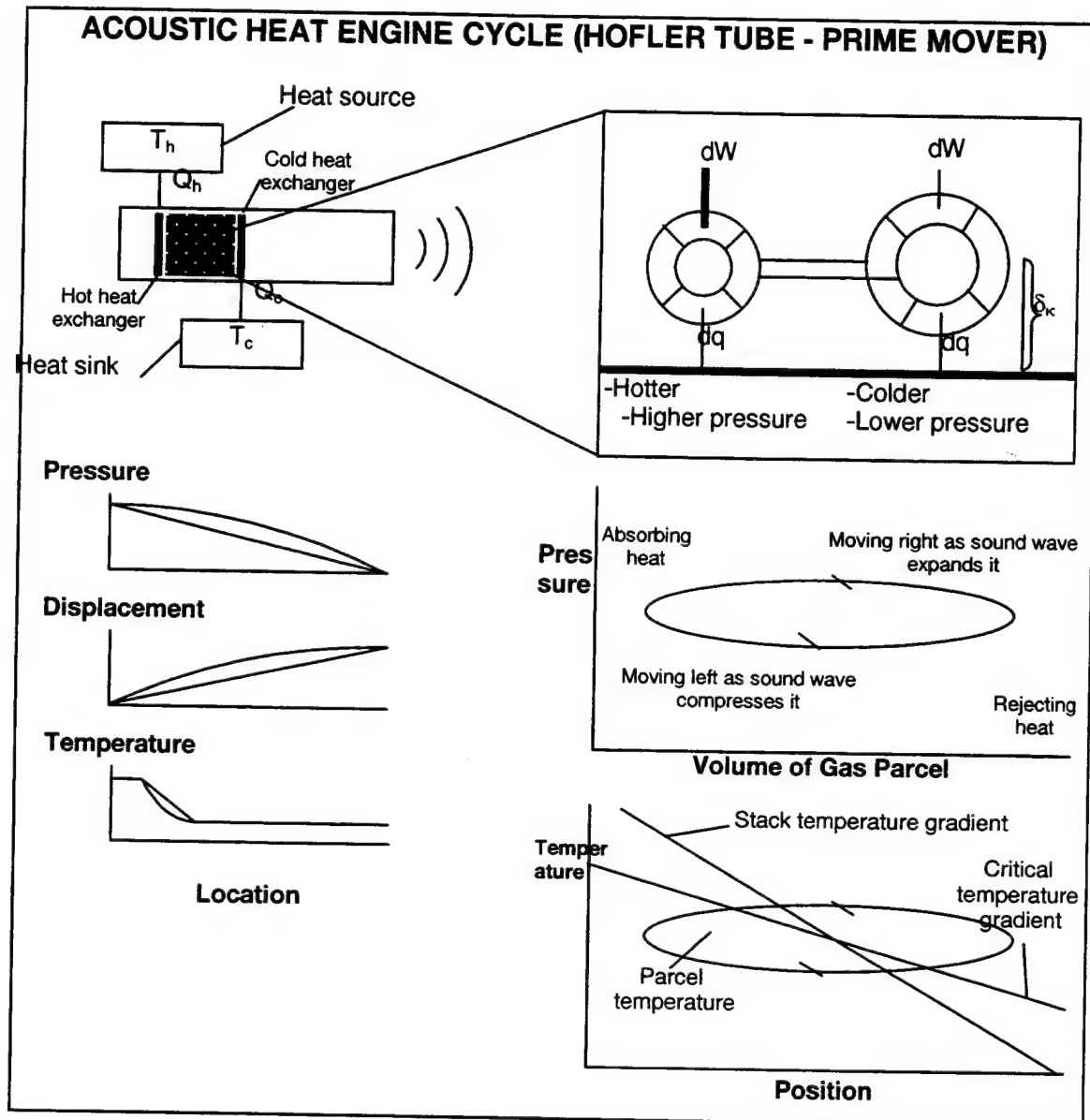
Figure 2.4 The Thermoacoustic Cycle: Shown is the cycle undergone by one infinitesimal parcel of gas. (a) The parcel adiabatically expands and moves to the right, away from the increasing acoustic pressure. (b) The parcel rejects heat energy to the cooler stack plating. (c) The oscillating acoustic pressure compresses the parcel and drives it back to the left. (d) The parcel absorbs heat energy from the hot stack plate. (From: Swift, 1995, pp. 22-28).

to the right, while at the same time the parcel absorbs heat from the plate.

The combination of the decreasing acoustic pressure and the increasing

17

temperature of the parcel causes parcel volume to increase during movement to the right.

While moving toward the cooler portion of the stack plating, the parcel begins to release heat energy into the plate. The oscillating acoustic pressure creates a region of reverse high-pressure gradient at this point, driving the parcel back to the left toward the region of high temperature while at the same time compressing the parcel.

Upon returning to the initial point at which the cycle began, the parcel is in its initial state and begins the cycle again. Each iteration of the cycle causes a small amount of heat energy to be transferred from the region of high temperature to the region of low temperature.

3. The Rott Wave and Energy Flow Equations

The Rott equations give a quantitative description of the thermoacoustic engine. (The derivation of these equations is provided by Swift (Swift, 1988, pp. 1145-1179), and due to their complexity, will not be presented here.) These equations, as modified by Swift, form the foundation of numerical models of thermoacoustic devices such as the Design Simulation for Thermoacoustic Research (DSTAR).

Rott developed the first equation for acoustic propagation within a channel formed by parallel plates, where the plates may have a temperature gradient. This equation, modified by Swift, serves to describe the acoustic

wave within the stack, which is closely approximated by such a channel (Wheatly, Swift, Migliori, 1986, pp.2-29; Swift, 1988, pp. 1145-1179), and is given by

$$\left(1+\frac{(\gamma-1)f_\kappa}{1+\varepsilon_s}\right)p_1+\frac{\rho_m a^2}{\omega^2}\frac{d}{dx}\left(\frac{1-f_\nu}{\rho_m}\frac{dp_1}{dx}\right)-\beta\frac{a^2}{\omega^2}\frac{f_\kappa-f_\nu}{(1-\sigma)(1+\varepsilon_s)}\frac{dT_m}{dx}\frac{dp_1}{dx}=0 \quad (2.10)$$

where

$$f_\nu=\frac{\tanh[(1+i)y_0/\delta_\nu]}{(1+i)y_0/\delta_\nu}$$

$$f_\kappa=\frac{\tanh[(1+i)y_0/\delta_\kappa]}{(1+i)y_0/\delta_\kappa}$$

$$\varepsilon_s=\frac{\sqrt{K\rho_m c_p}\ \tanh[(1+i)y_o/\delta_\kappa]}{\sqrt{K_s\rho_s c_s}\ \tanh[(1+i)y_o/\delta_s]}$$

$$\sigma=c_p\mu/K=\nu/\kappa$$

$$\delta_\kappa=\sqrt{2\kappa/\omega}$$

$$\delta_\nu=\sqrt{2\nu/\omega}$$

Here, σ is Prandtl number, δ_κ is thermal penetration depth, δ_s is the viscous penetration depth, f_ν is the coefficient for the viscous boundary layer in the gas, f_κ is the coefficient for the thermal boundary layer in the gas and ε_s the coefficient for the interaction between thermal boundary layers in the gas and the solid. The last three coefficient are the integrals over the thickness of the boundary layer.

The above equation is a general form that is applicable for both liquids and gases as the propagation medium. However, if the medium is assumed to be an ideal gas, the ideal gas law may be applied. This, combined with the

19

definition of a set of non-dimensional state variables, reduces Equation (2.10) to

$$\left[1+\frac{(\lambda-1)f_\kappa}{1+\varepsilon_s}\right]\mathbf{P}+\left[(1+f_\nu)+\frac{1}{2}(1+\beta_r)(f_\nu+\tanh^2\eta_0-1)-\frac{f_\kappa-f_\nu}{(1-\sigma)(1+\varepsilon_s)}\right]\frac{d\mathbf{T}}{d\mathbf{X}}\frac{d\mathbf{P}}{d\mathbf{X}}+(1-f_\nu)\mathbf{T}\frac{d^2\mathbf{P}}{d\mathbf{X}^2}=0 \quad (2.11)$$

where

$$\eta_0=(1+j)(y_0/\delta_\nu). \quad (2.12)$$

The capitalized, bold-faced variables are normalized or non-dimensional variables, and are defined in Appendix A. Equation (2.11) allows the complex state variables of pressure and pressure gradient or velocity to be determined if the temperature gradient is known.

The second parameter of interest for the development of thermoacoustic models is the 2nd order enthalpy, H_2. This energy flow equation, as developed in Ref [5] is

$$\begin{aligned}
\dot{H}_2 &= \frac{\Pi y_0}{2\omega\rho_m}\text{Im}\left[\frac{d\tilde{p}_1}{dx}p_1\left(1-\tilde{f}_\nu-\frac{T_m\beta(f_\kappa-\tilde{f}_\nu)}{(1+\varepsilon_s)(1+\sigma)}\right)\right] \\
&+\frac{\Pi y_o c_p}{2\omega^3\rho_m(1-\sigma)}\frac{dT_m}{dx}\frac{dp_1}{dx}\frac{d\tilde{p}_1}{dx} \\
&\times\text{Im}\left[\tilde{f}_\nu+\frac{(f_\kappa-\tilde{f}_\nu)(1+\varepsilon_s f_\nu/f_\kappa)}{(1+\varepsilon_s)(1+\sigma)}\right] \\
&-\Pi(y_0 K+lK_s)\frac{dT_m}{dx}
\end{aligned} \quad (2.13)$$

The final local state variable of temperature can be determined by DSTAR with Equation 2.14. If the energy equation is rearranged to express the temperature derivative with respect to position in terms of the constant

enthalpy term and acoustic variables, and an ideal gas law and non-dimensional variables are used, the result is:

$$\frac{d\mathbf{T}}{d\mathbf{X}} = \frac{\mathbf{T}\,\mathrm{Im}\left[\dfrac{d\tilde{\mathbf{P}}}{d\mathbf{X}}\mathbf{P}\left(1-\tilde{f}_{v}-\dfrac{f_{\kappa}-\tilde{f}_{v}}{(1+\varepsilon_{s})(1+\sigma)}\right)-\mathbf{H}_{2}\right]}{\dfrac{\mathbf{T}}{(\lambda-1)(1-\sigma)}\left|\dfrac{d\mathbf{P}}{d\mathbf{X}}\right|^{2}\mathrm{Im}\left[1-\tilde{f}_{v}-\dfrac{(f_{\kappa}-\tilde{f}_{v})(1+\varepsilon_{s}f_{v}/f_{\kappa})}{(1+\varepsilon_{s})(1+\sigma)}\right]+\mathbf{K}}$$

(2.14)

With the development of the wave and energy equations described above, mathematical techniques must be used to determine the solutions applicable to the device of interest. To properly solve the equations as initial value problems or boundary value problems, numerical techniques must be used since closed form solutions are not available.

21

THIS PAGE INTENTIONALLY LEFT BLANK

III. ASSEMBLY OF SINGLE DISK DRIVER (SN-01)

The mini TAR driver is composed of three main parts: the top plate, the bottom plate and the driver body (sidewall). Each part includes smaller components. This chapter describes in detail the assembly of the main parts as well their smaller components.

A. ASSEMBLY OF FRONT (TOP) PLATE

The top plate is one of the three main parts of the mini TAR driver. The top (or front) plate is one of the most critical and important part of the driver, because this plate contains both the piezo disk and steel diaphragm. Acoustic power is produced by this plate, and is delivered to the resonator.

In Fig.3.1, the design of top plate is shown. Professor T. Hofler is the designer of the stainless steel foil disk and push rod attachments. The piezo disk is attached to the push rod by using epoxy EC2850FT. Epoxy EC2850FT is used because this adhesive is electrically insulating. The epoxy fill material consisting of tiny glass particles provides the insulating characteristics.

Another important part of top plate is the capillary tube, which is required for static pressure equalization. This tube provides the gas transfer between the driver and the resonator. The diameter of the capillary tube is very crucial. If the diameter is too big, it will reduce the dynamic acoustic pressure. If the diameter is too small, then there will be little pressure

Mini Driver Top
Make 5 of 6061-T6 Aluminum
Notes: X.XXX tolerance is ± 0.003"; X.X° tolerance is ± 0.05°.

Tom Hofler
Physics
Room SP-142
X-2420
tjhofler@nps.navy.mil

Top View

B'

22.5°

A'

A

B

tapped 2-56,
8 eq. spaced places

0.143" ± 0.002"
diam. counterbore

drill #43 thru,
8 eq. spaced places

3/64" wide groove, 0.020" deep

Section A - A'

1.570"±0.002"

0.325" — 0.532"

0.063"

0.090"

0.170"

0.286"

0.125"

0.112"

1.760"

Section B - B'

1.150"±0.002"

0.454"±0.001"

0.140"

0.354"±0.002"

3/64" wide groove, 0.020" deep

drill #60 thru

Bottom View

44 drill

drill # 60 thru
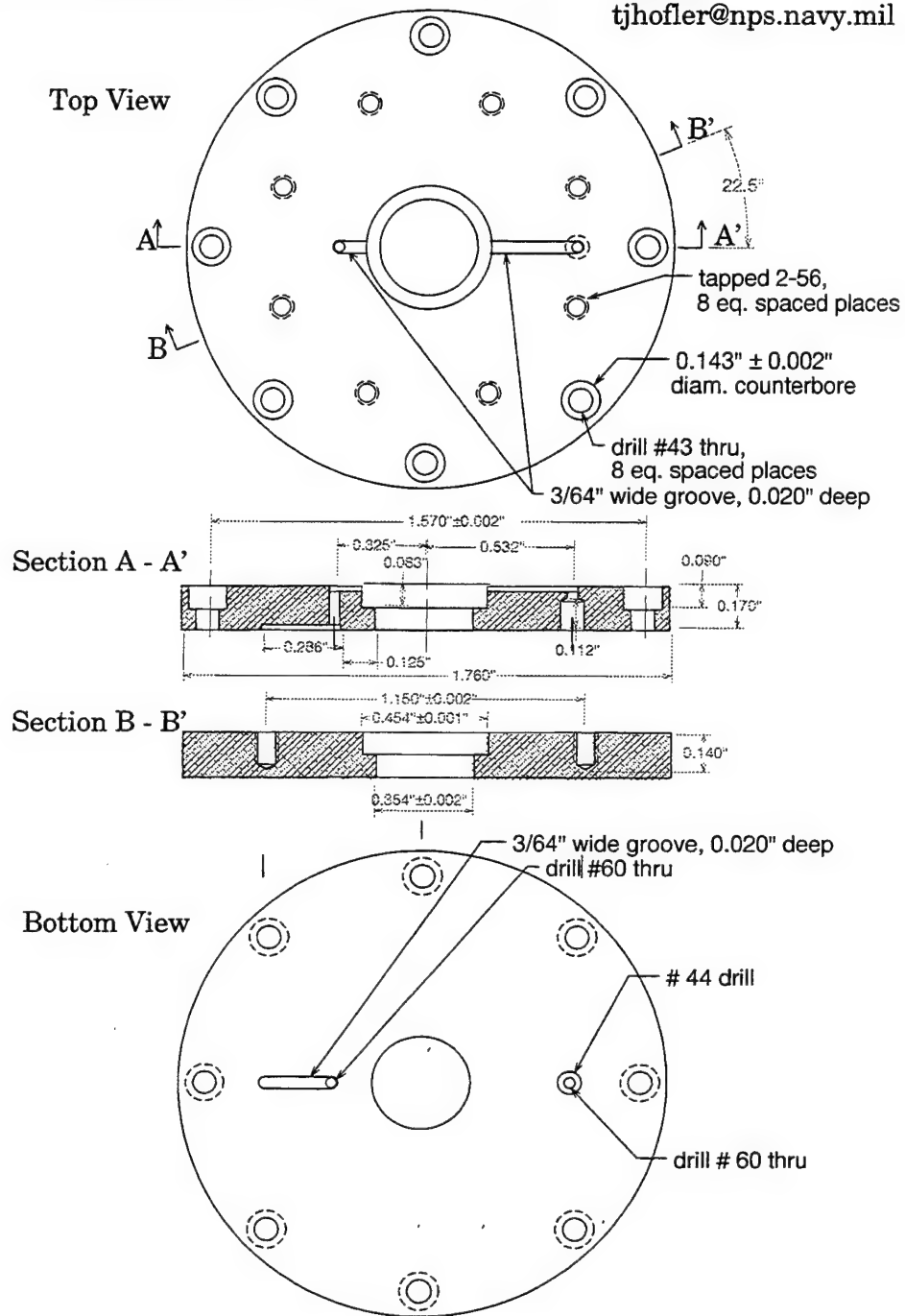
Figure 3.1. The design of the top plate

24

equalization and pressure differentials may then exceed levels that are safe for the thin steel diaphragm. If the diameter is too small, then there will be little pressure equalization and pressure differentials may then exceed levels that are safe for the thin steel diaphragm.

Thus, during manufacturing special care must be taken to ensure the capillary tube's functionality. Also, special care must be taken to avoid blocking the capillary tube while gluing it to the top plate. For more information about the installation and production of capillary tube, see Livvarcin, 2000 [ref 9].
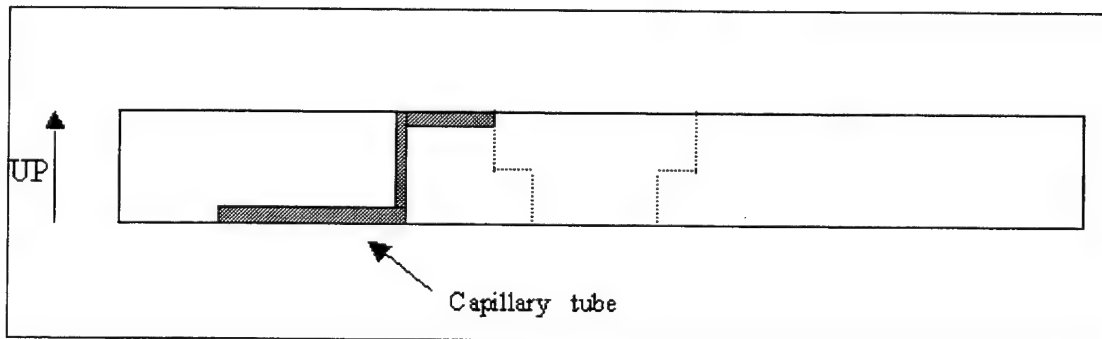
Figure 3.2. The capillary tube used for pressure equalization. (Livvarcin, 2000, pp. 70)

B. ASSEMBLY OF BOTTOM PLATE

There are four holes on the surface of bottom plate. Two of them are for electrical feed-throughs for the power amplifier signal, one electrical feed-through for a microphone cable, and the other is for injecting the desired amount of gas into the mini TAR driver.

25

Two mini banana jacks are installed onto the bottom plate for the power amplifier connection. These mini banana jacks are gold plated with solder terminals on the backside. Two small pieces of wire are soldered to the legs of banana jacks to provide a connection between banana jacks and the piezo disk. Before installing the banana jacks to the bottom plate, the jacks are painted with 2850FT epoxy, placed in the holes, and these holes are filled with 2850FT epoxy. 2850FT epoxy is used for two reasons. First, the epoxy prevents electrical conductivity between the banana jacks and the plate. The other reason is that the epoxy prevents gas leakage.

After installation, electrical continuity is checked periodically until the epoxy has cured. During these checks, the electrical resistance is found to have been between 100 KΩ and 1 MΩ. Although this resistance means there is conduction, this amount of conduction is typical of ionic transport in the wet epoxy and disappears when the epoxy is fully cured.

{While the discussion of the connectors and microphone below is OK, the rest of the discussion concerning the analyzer and test resonator should be reserved for a section or chapter on the test resonator measurements.}

The microphone connector and microphone are used to find the resonant frequency, dynamic pressure ratio, response of the resonator to driven voltage, and to calculate pressure. During the test resonator measurements, (explained in detail in Chapter V), the microphone is connected to an SRS785 two-channel dynamic signal analyzer. With the

SRS785 signal analyzer the mini TAR is driven in swept sine mode at various amplitudes under varying amounts of static gas pressure.

The frequency span during measurements is taken between 3.5 kHz and 5.5 kHz. The resonant frequency of the system is always within this frequency span. To obtain the optimal response of the test resonator, various plunger positions, driven voltages, and driven pressures are used. As previously explained, the microphone is used just for scientific development purposes; for large-scale production, the microphone can be eliminated.

The installation of the microphone feed-through is more complex than the installation of the power amplifier feed-through. All four-microphone uninsulated copper wires pass through one hole. Because insulated wires will cause gas leakage. During installation, these four wires must not touch each other in the hole and create electrical shorts. They are held with a small separation from each other using a four-terminal connector and 2850FT epoxy.

C. ASSEMBLY OF DRIVER BODY

The third part of driver is the driver body, which has a hollow cylinder shape. There are no subparts on the surface of the body. The body's function is to create a sealed cavity between the top plate and the bottom plate, and to make space for the piezoelectric components, the microphone and the wiring.

D. FINAL ASSEMBLY

The last phase of assembly is the attachment of top, bottom and body to each other. Before attaching these parts, the power wires are soldered to the piezo disk, and the microphone wires are soldered to the microphone. Each plate contains eight holes for screws that will serve to secure the parts together, establishing a good rubber O-ring seal to prevent gas leakage. The driver's top plate also will connect to the resonator with eight screws. A Teflon gasket is used to prevent gas leakage between the driver and resonator.

Finally, the construction and assembly of a fully pressurized acoustic driver with dynamic pressure transducer was partially completed.

While the ultimate miniaturization of the driver is constrained by the diameter of the PZT disk component, the driver, which is given above is considerably larger than a finalized production unit would be. There are two reasons for this. First, a dynamic pressure transducer has been included inside the driver. The overall outer diameter was increased moderately to accommodate the transducer and the overall length of the driver was increased greatly to accommodate both the transducer and the hermetic transducer pressure feed-throughs. In a production unit the pressure transducer would likely be absent.
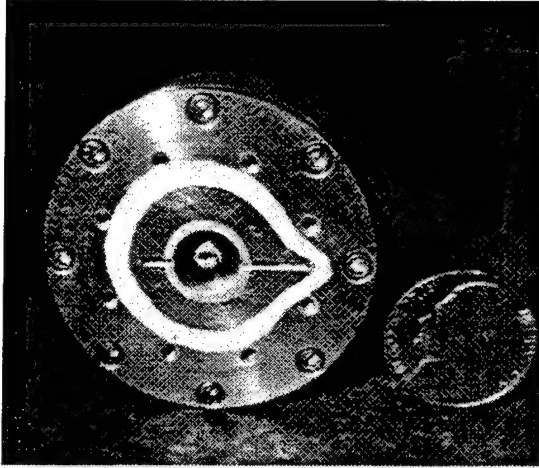
Figure. 3.3a Driver #1 diaphragm view
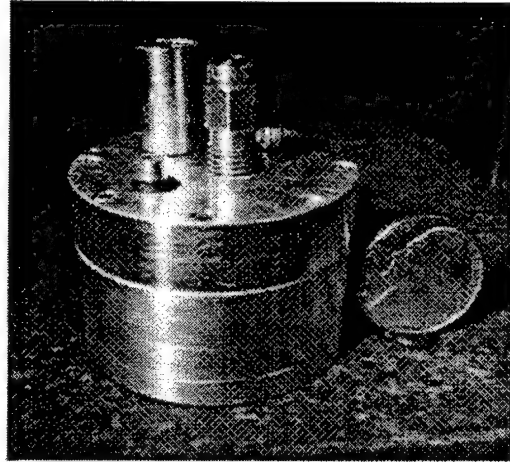
Figure. 3.3b Driver #1 feedthrough plate view

THIS PAGE INTENTIONALLY LEFT BLANK

IV. TEST RESONATOR

A. PURPOSE

Before constructing the steel mini TAR resonator, a copper test resonator is created as a substitute for the steel mini TAR resonator. This copper test resonator operates with pure noble gas over a wide range of static pressures. Depending on the static pressure this test resonator can provide an acoustic load on driver similar to that of the mini TAR resonator. Fig. 4.1 shows the design of the test resonator.

The test resonator consists of a tube that can be hermetically coupled to the driver and closed at the opposite end with an adjustable piston having a sliding seal. High amplitude standing waves in constant cross-section tubes usually generate large amounts of harmonic distortion and shock waves. The bore of the tube was shaped in a manner somewhat similar to the real refrigerator resonator.

Displacement measurement is critical in understanding the behaviors of the driver. By knowing the size of the displacement and generated force, it is possible to calculate the pressure and power produced by the driver.

The test resonator is used because the construction of the steel mini TAR is not yet finished. It is much simpler to fabricate than an optimal TAR resonator and expetide the experimental phase of this project—it has been designed with the aid of DSTAR, and is used in measurements.

31

The refrigeration hardware will not be assembled for some time, since its performance characteristics are less certain and more variable than for a test resonator. Finally, a test resonator is easier to adjust in frequency.

Using the SRS785 signal analyzer and test resonator, the performance of the driver has been tested. Before installing the steel mini TAR resonator, the driver's performance should be tested to determine if the driver produces enough power.

For example, according to the measurements discussed in Chapter.V, the driver with one single piezo disk does not produce enough force or acoustic power to produce significant amounts of refrigeration with the mini TAR resonator. Potential modifications for improving the performance of the driver are discussed in Chapter V.

Also, the impedance matching of the resonator and driver can be investigated by using an SRS785 signal analyzer. The data, taken with the signal analyzer, can be used to determine the best resonator gas pressure and acoustic impedance for optimal acoustic power generation.

Another purpose for the test resonator is to adjust the length and its resonant frequency to find the optimal operating frequency of the mini TAR driver. Since the copper test resonator has an adjustable plunger, the optimal length and resonant frequency can be found for a driven voltage and pressure amplitude.
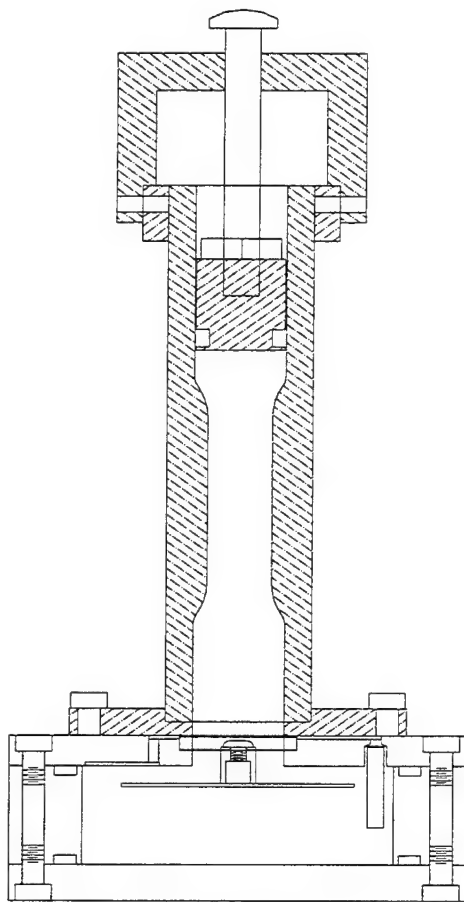
Figure 4.1. The test resonator shown attached to a single disk driver.

In order to determine the precise resonance frequency of the resonator, it is necessary to obtain the maximum acoustic pressure amplitude. Since both the piezo disk and the resonator are independently resonant, for best power and efficiency, two resonance frequencies should be matched to each other. Also, during measurements it has been observed that the resonant frequency of the piezo disk changes slightly with the magnitude of the driven voltages.

Theoretically, the fundamental resonance of the test resonator is effectively one half of a wavelength. The resonant frequency of the piezo disk was found as 4300 Hz. From the following equations, the wavelength can be calculated:

$$\lambda = \frac{c}{f} = \frac{344 \, m/s}{4300 \, Hz.} = 0.08 \, m = 80 \, mm \tag{4.1}$$

and one half of a wavelength is,

$$\frac{\lambda}{2} = \frac{0.08}{2} \approx 0.040 \, m = 40 \, mm \tag{4.2}$$

As previously mentioned, for optimum performance, the acoustic impedance of the driver and the resonator tube must be matched. This matching process may cause the resonant frequency of the combined system to be slightly different than the two of independent resonant frequencies.

B. DESIGN WITH DSTAR

An obvious test resonator design would use a straight tube for which the resonant frequency can be adjusted easily. The hope is that the standing wave does not become nonlinear at the high-pressure amplitudes of interest. There are some reasons why the dynamic pressure becomes nonlinear in a straight tube.

If the tube is a rigid-rigid terminated straight tube, standing waves can be excited in two ways. One way is by designing the tube such that one

end is caused to vibrate slightly and is thus not exactly rigid, which causes standing waves to be excited. Another way is by shaking the tube back and forth in the axial direction to excite standing waves.

In our measurements, the peak pressure is as high as 4% or 5% of the mean pressure (Po/Pm = 5%). A 1% level in a straight resonator tube with rigid or nearly rigid terminations at both ends will typically display a substantial distortion in the pressure waveform. The reason for this distortion is the fundamental acoustic non-linearity of to the gas itself or of the wall interaction.

The amount of distortion production in one acoustic cycle is quite small at these amplitudes. However, if the harmonic frequencies of these nonlinear processes lie exactly on top of the resonant frequencies of the higher modes of the resonator, then the result is a big distortion. The small inherent distortion products are amplified by the quality factor of these higher modes.

Some resonators exhibit large amounts of distortion and some do not. The key issue for the critical difference between resonators is the exact resonant mode frequency structure. If we have a second mode frequency, which has exactly doubled the fundamental frequency, then the harmonic distortion of fundamental frequency can create the frequency that exactly matches the second resonant mode frequency. Some resonators exhibit this matching property, and some do not. A straight resonator tube possesses this property.

35

When we look at the mini TAR driver, which is pressurized with a stainless steel disk, the acoustic impedance is roughly that of a rigid-rigid terminated tube. So a test resonator constructed with a straight tube will result in a large distortion. In order to prevent this distortion, a new resonator, whose hour-glass shape enables the resonant mode frequencies of the tube to be shifted, has been developed by Dr. Thomas Hofler.

Since the middle of the resonator is narrow, the right adjustment must be made for resonant frequency because the plunger cannot enter the tube anymore. Now, we have a limited adjustment range for the fundamental resonant frequency.

At this point DSTAR plays a very important role. The fundamental resonant frequency is shifted downward substantially by the hour-glass shape, and obtaining the correct adjustable frequency band is essential. Furthermore, the amount of diameter change in the hour-glass shape should be enough to suppress distortion, but no more. Very large diameter changes will cause excessively high acoustic velocities and other nonlinearities associated with high velocity.

The exact shape the resonator tube has been designed and put into the DSTAR. With DSTAR, the exact resonant frequency can be calculated when the plunger is in any position. Also, with DSTAR, not only can the fundamental frequency be modeled, but also the second mode, third mode, and so on. Fig. 4.2 shows a calculation of a resonant solution with DSTAR.

36

The frequency of the 2nd mode is determined to be 2.625 times greater than for the fundamental mode. This is substantially different than either a 2nd harmonic distortion frequency or a 3rd harmonic distortion frequency.

Since the test resonator can be operated over a wide range of static pressures, a wide range of acoustic load impedances can be obtained for driver testing. The acoustic load impedance at the resonant frequency, $Z(f_o)$, is approximately proportional to the product of mean gas pressure and the quality factor Q. The Q is proportional to the square root of the mean pressure. So overall,

$$Z(f_o) \propto p_m Q \propto p_m^{3/2}.$$

Since the test resonator does not have a thermoacoustic stack in it, it generates the same acoustic load impedance at a mean pressure of 10 bar that the refrigerator resonator would generate at a mean pressure of 15 bar. This factoid is based solely on DSTAR calculations.

Local State Quantities

SimpTube3FixLen.tae
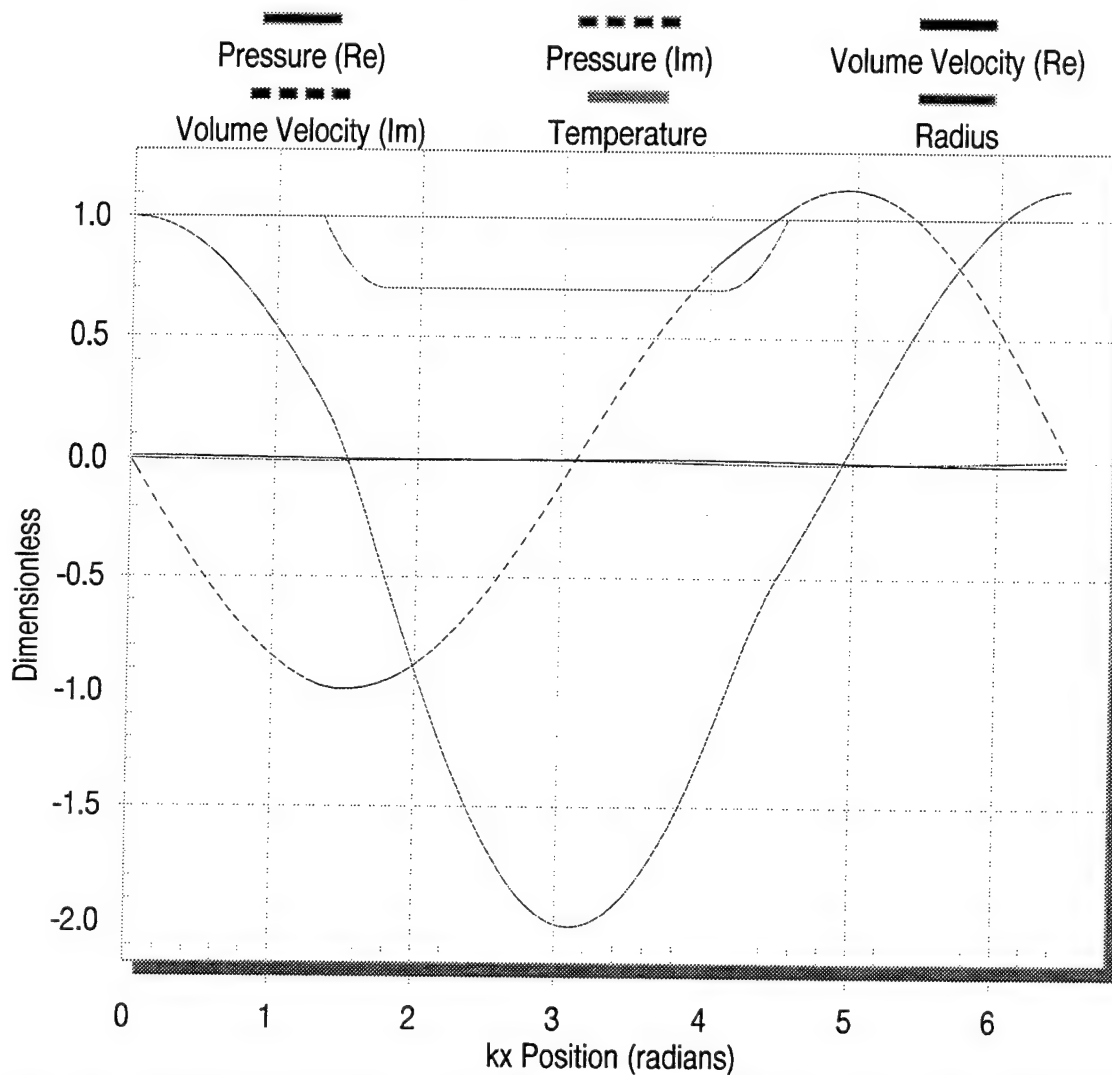
Figure 4.2. Graphical solution of the 2nd mode of the test resonator calculated with DSTAR. The frequency of the 2nd mode is 2.625 greater than the fundamental mode.

38

V. MEASUREMENTS WITH SINGLE DISK DRIVER AND TEST RESONATOR

The main purpose of the driver is to produce the acoustic power required for cooling. The piezoelectric disk produces vibration power, and the stainless steel diaphragm converts this power into a useful acoustic form. The acoustic power is delivered to the resonator tube.

The flexibility and dimensions of the steel diaphragm are critical to achieve the maximum generation of acoustic power. If the diaphragm is too flexible, acoustic power will be lost due to the high impedance acoustic pressures being generated in the resonator. The high impedance will force portions of the soft diaphragm to move in opposite directions, negating some or most of the net volume displacement. If the steel diaphragm is too rigid, the piezoelectric disk may not produce a sufficiently large linear displacement amplitude.

In order to obtain the maximum amount of acoustic power, the flexibility of the steel diaphragm must be in the correct range of values.

A. BACKGROUND FROM LIVVARCIN THESIS

In order to better understand the characteristics of the driver being developed in this thesis research, some of Livvarcin's preliminary driver data is discussed here. The data in Livvarcin's research is obtained using a single disk driver with a large paper cone and a plastic test resonator.

Livvarcins' working medium is air at 1 atm a variable determined by the plastic test resonator used. He finds peak acoustic pressure amplitudes that are 7% to 8% of the mean pressure of 1.014 bar at a 4 kHz resonant frequency. Figure 5.1 shows the plastic test resonator used in his measurements. This is a "closed-end open-end" quarter wavelength resonant tube with the coupling to the large paper cone approximating an "open-end" of the tube. For more information about his test resonator, see Ref 9.

The measurements made are swept sine transfer functions of pressure response relative to the drive voltage, performed at low amplitudes. Several measurements are taken by varying the resonator length. The highest peak in the pressure transfer function is obtained with a tube length of 20.4 mm at a frequency of 4.075 kHz. A graph of this transfer function is shown in Fig.5.2.
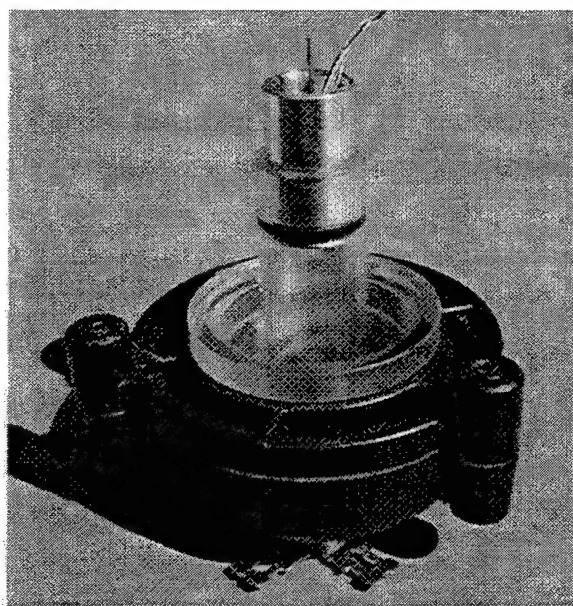
Figure 5.1. The test resonator and piezo driver, 5.8 cm in total length
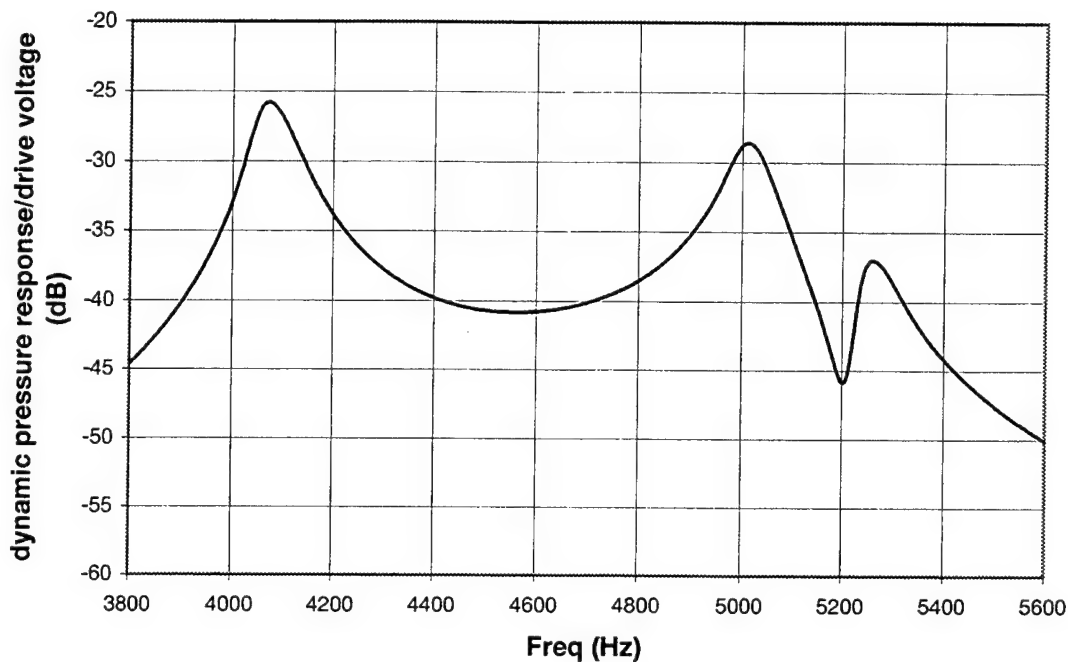
Figure 5.2. Test resonator dynamic pressure response curve. Pressure sensor sensitivity is 280.0 mV/psi

The second group of test resonator measurements Livvarcin makes determines the pressure response linearity, hysteresis and maximum amplitude of this test resonator system. For this experiment, the starting voltage amplitude is 0.25 V rms, is increased to 15 V rms, and then decreases back to 0.25 V rms. The drive frequency is adjusted for maximum pressure response for each data point during measurement. The measurement shows that the response hysteresis is less than a 3%, which is not significant.

The following graph shows the measured voltages with a microphone placed in the tube. The dashed line shows the measurement during the increment, and the solid line shows the measurement during the decrement.
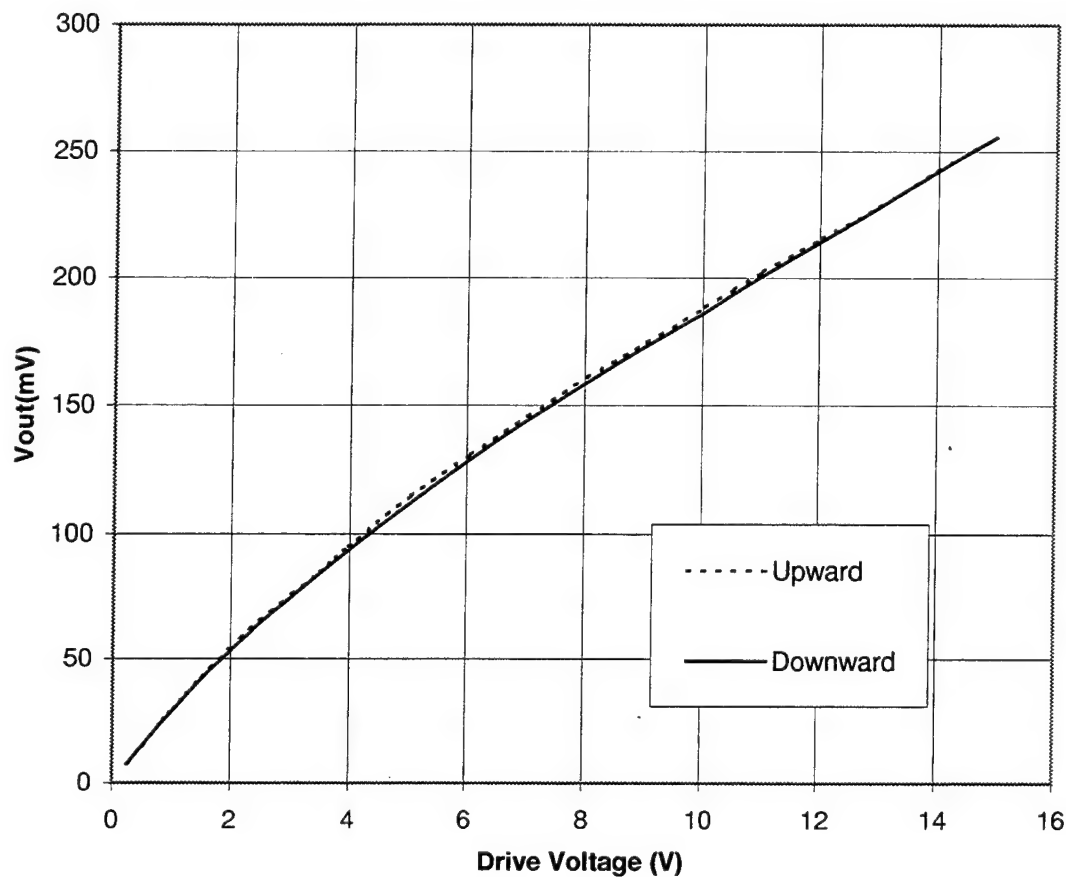
Figure 5.3. Input voltage vs. output voltage at the microphone

Also observed is that the resonant frequency of the driver and resonator system decreases by roughly 4% at the highest amplitudes compared to the lower amplitudes. A moderate amount of response nonlinearity is seen in Fig. 5.3. It is smooth function of amplitude and it is likely that it represents the characteristics of the piezoceramic material.

Livvarcin took the next sets of measurements with the first high acoustic impedance driver having a single peizoceramic disk and a steel diaphragm. At the time, the assembly of this driver was mostly completed, but could not be pressurized.

Driver diaphragm displacement measurements are made using a laser vibrometer and sound level meter having an analog output signal. For these measurements, the driver is not coupled to a resonator and the diaphragm simply radiates out into the room. Due to the range limitations of the laser vibrometer, it is impossible to make measurements at high drive voltages where the vibration response exceeds the range of instrument.

Also, with the sound level meter, the sound level produced by the driver must be much higher than the ambient noise level in the room. Otherwise, the test results may be invalidated by extraneous ambient noise. This is not difficult to achieve if the sound level meter is placed very close to the steel diaphragm of the driver.
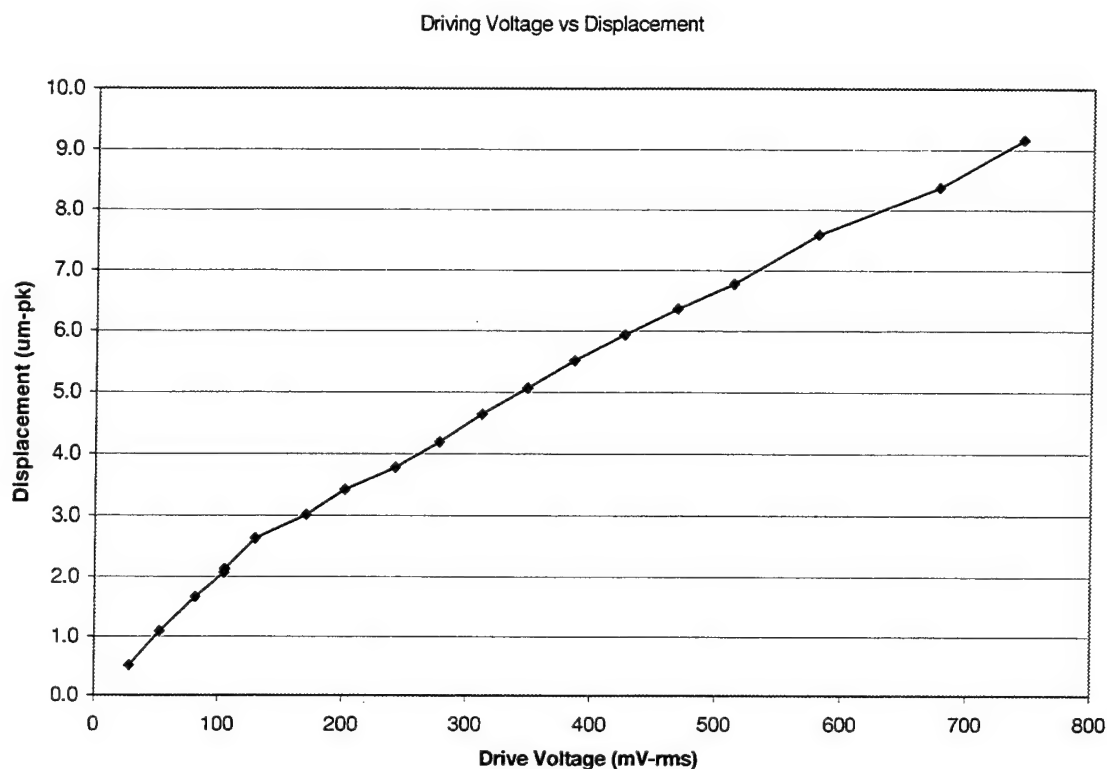
Figure 5.4. Displacement measurements with laser vibrometer

Since the main purpose of this measurement is to check the linearity of the driver response, the measured output voltages are not converted to an absolute sound pressure scale. The following graph shows the output response of the mini TAR driver in terms of microphone signal versus driving voltages.

From the Fig. 5.5, it is notable that the measurements are roughly linear up to 4 V rms and a rather abrupt nonlinearity starts at 5 V rms.

Since the frequency response of the driver gives information about the general response of the driver, these measurements are also made by Livvarcin, and the Fig. 5.6 shows the result for a 146 mV rms driving voltage.
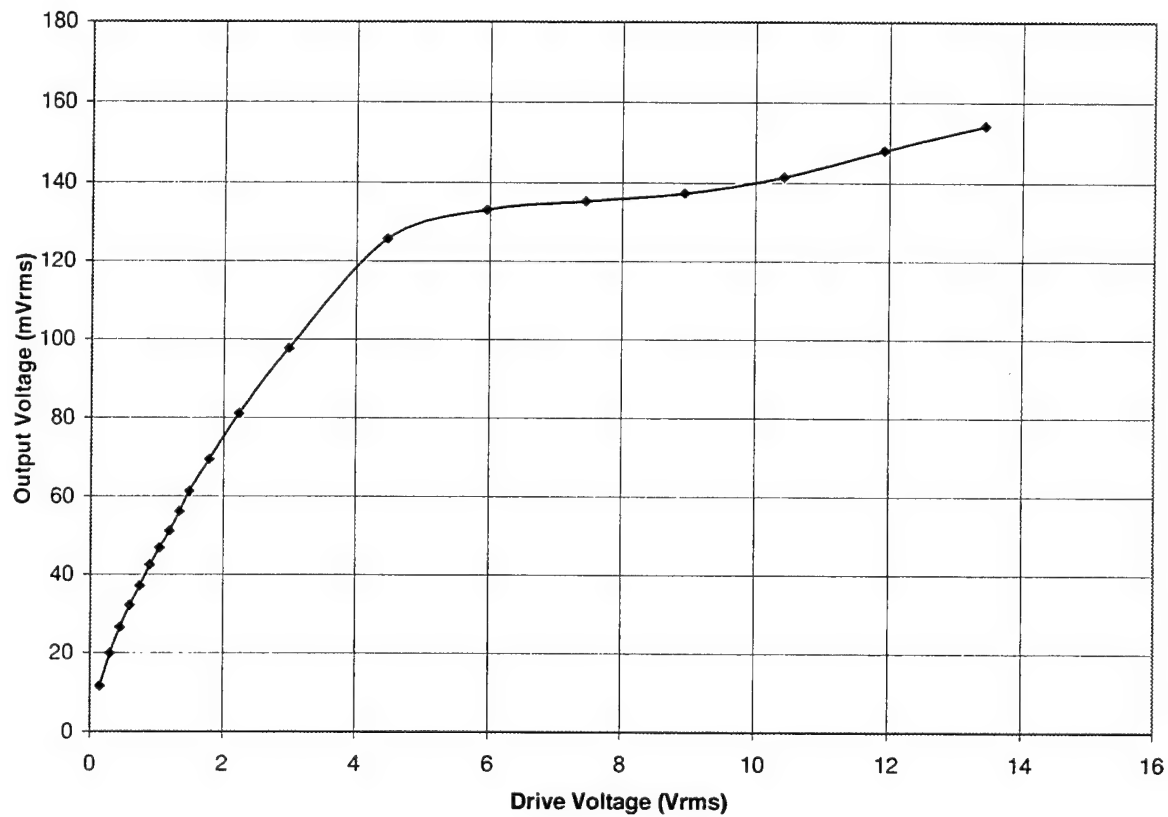
Figure 5.5. Sound pressure response measurements of the mini TAR driver
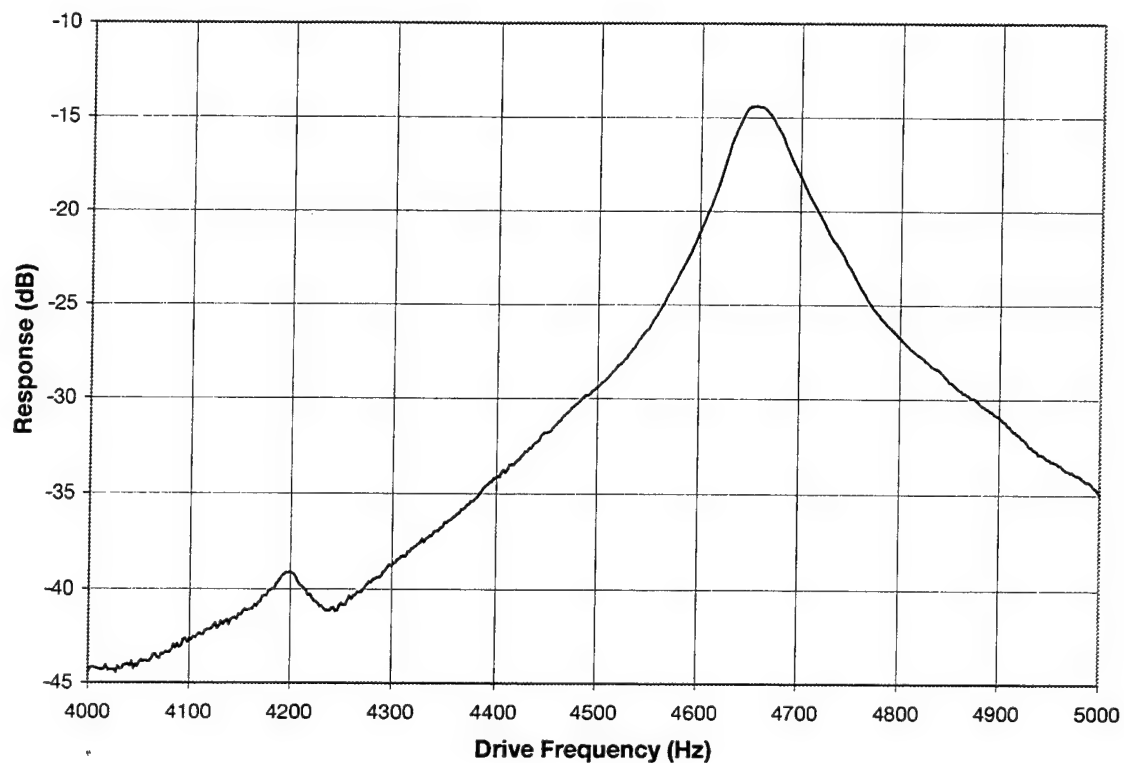
Figure 5.6. Frequency response of the driver at 146 mVrms driving voltage
(Microphone measurements)

A very substantial and abrupt hysteresis is shown in Fig. 5.7 below for
the frequency response measured at high driver amplitude. The drive
frequency is swept upwards for one curve and downwards for the other.
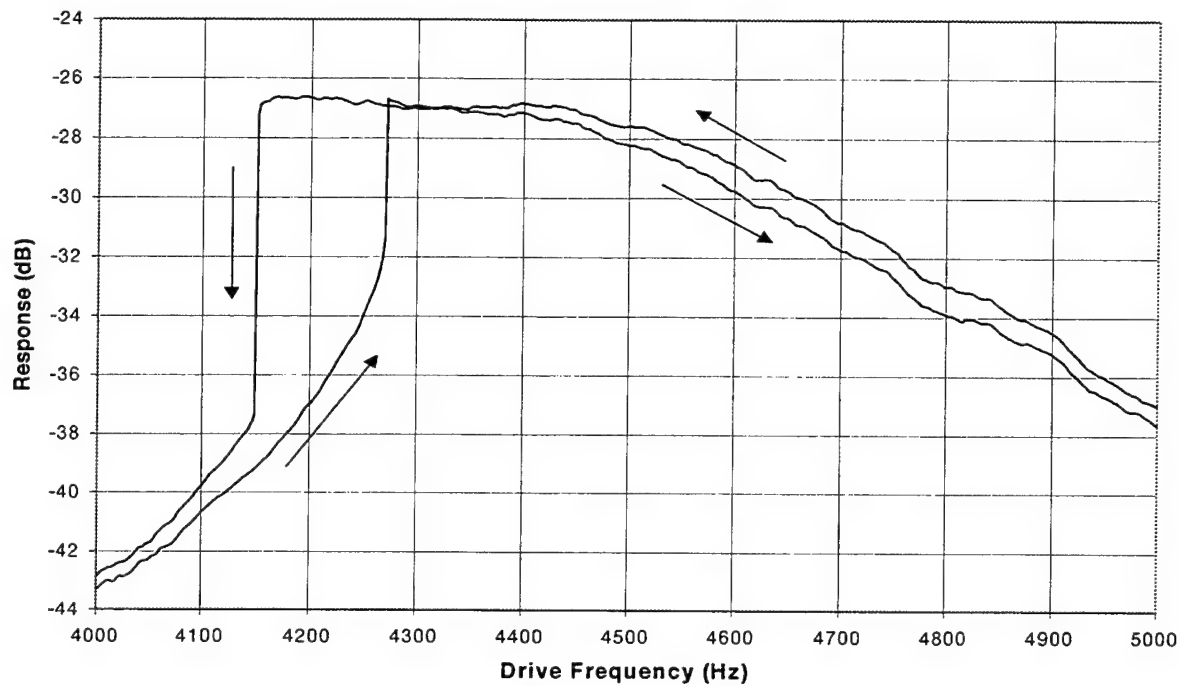
Figure 5.7. Frequency response (with the microphone) of the driver at 8.75 Vrms driving voltage

B. MEASUREMENT SETUP FOR DRIVER WITH TEST RESONATOR

After installing the completed mini TAR driver SN-01 with the test resonator discussed in Chapter IV, a variety of measurements were taken. For this purpose, an SRS785 two-channel signal analyzer, two multimeters, a preamplifier, a power amplifier, and a gas panel system are used. The system's setup is illustrated in the following figure.
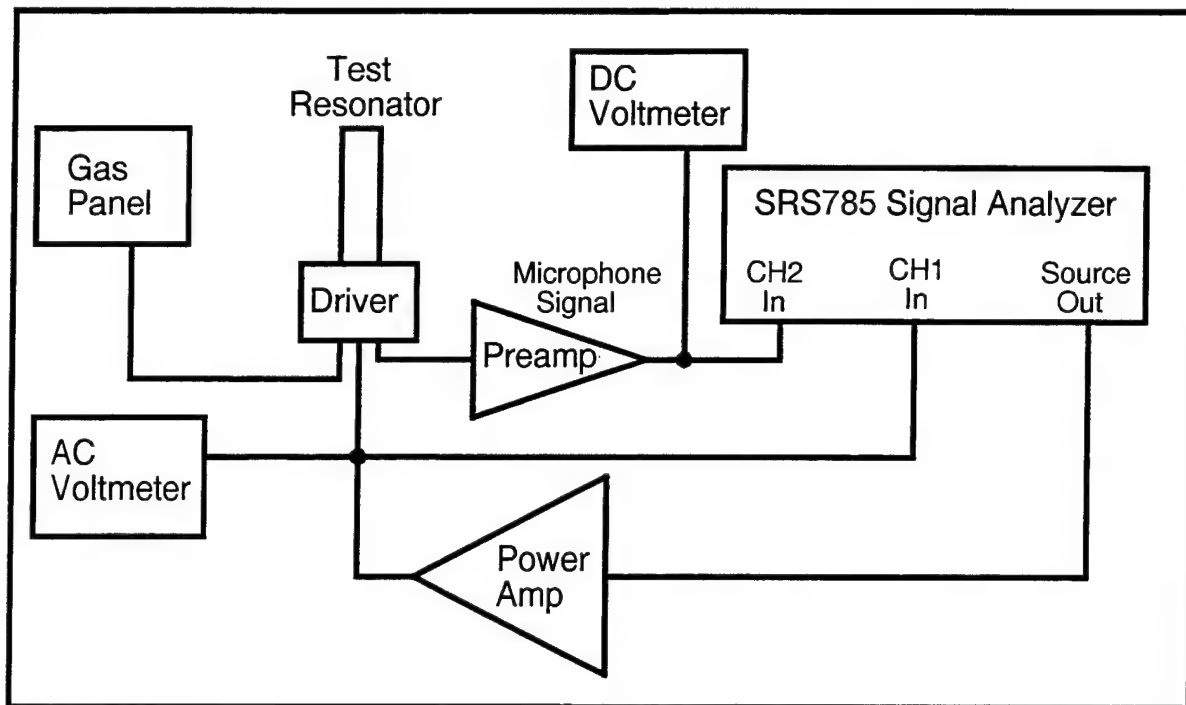
Figure 5.8. The measurement setup

For a low drive voltage amplitude, the driver can be driven by an signal analyzer. Since the signal analyzer can drive the driver up to an amplitude of only 5 V rms, a power amplifier is needed for higher voltage amplitudes.

The signal analyzer is very useful for the test measurements. With the help of the signal analyzer operating in swept sine mode, the resonant frequency of both the driver and resonator can be measured. The matching resonant frequencies and the dynamic pressure response of the system can also be measured.

The SRS signal analyzer sweeps the drive frequency either up or down. The sweep frequency span and drive voltage can be adjusted very easily. The

data is taken and saved to a diskette for later storage, viewing and plotting with a desktop computer.

The microphone contained inside the mini TAR driver is connected to a custom preamplifier. The microphone used is an Endevco model 8514-10. With the help of the microphone, the absolute pressure amplitude developed inside the test resonator can be measured. The resonances of both disk and test resonator can be seen in the frequency response sweep and hopefully matched by tuning the adjustable test resonator. The frequency matching process will maximize the acoustic power delivered to the resonator.

One of the multimeters is connected to the microphone preamp and used in DC voltage modeto check the pressure difference across the steel diaphragm while pressurizing or depressurizing the system. A maximum mean pressure difference of 0.2 bars is enforced.

The maximum drive voltage for piezo disk is 15 Vrms. Damage begins to occur at 17 V rms. The other multimeter is used to check the AC drive voltage amplitude. Aided by this multimeter, damage to the piezoceramic is easily avoided.

C. INITIAL MEASUREMENTS

The measurements with SN-01 show that the driver performed qualitatively as expected, but with less acoustic amplitude than required for the refrigerator. All test resonator data shown in this thesis were taken with He-Ar gas mixture with Ar concentration at 18% atomic.

With the single disk driver and copper test resonator, the system tests begin with a medium of air at 1 atm. The purpose of this measurement is whether or not to check the system is working properly acoustically. This constitutes a simple systems check to ensure that the piezoceramic disk, microphone, and amplifiers are all functioning prior to pressurization.

The next step is to fill the driver and resonator system with pure helium-argon gas mixture. This is accomplished by means of a gas purge cycle that is repeated 4 times. A purge cycle consists of evacuating the system to a pressure of 1 or 2 psi absolute, followed by filling to a pressure of 80 to 100 psi absolute, followed by bleeding and evacuating down to 1 or 2 psia again.

Since the filling process typically takes 1.5 to 2 hours to complete, it is wise to begin the process with a simple leak check. Begin by filling the system with gas to 80 or 100 psi absolute, and then shut the fill valve while monitoring the pressure for 10 min. If the pressure drops by less than 0.5 psi over a 10 min. period, then the system is sufficiently leak-tight to complete the fill process and take measurements.

If there is any reason to suspect that the system is less than perfectly leak-tight, try to keep the time spent with the gas pressure below atmospheric to a minimum. Air may enter the system during prolonged evacuation periods.

The first issue is matching the frequency of the test resonator to the frequency of the driver's mechanical resonance. This is made more difficult because of the fact that the driver's resonant frequency drops substantially as the driver amplitude is increased, resulting in what is known as a "bent tuning curve. Figure 5.9 illustrates the frequency shifting of the driver resonance with amplitude, the bent tuning curves, and the ideal case where the two resonances are matched at the highest drive amplitudes for maximum acoustic power delivery to the resonator.

Numerous data are gathered at various plunger positions and various voltage amplitudes to find the optimal plunger position to match the two resonant frequencies of the system. 4630 Hz is the low amplitude driver resonance, which will move downward as the amplitude increases. 4270 Hz is the test resonator resonance, which is the important frequency that does not change with amplitude. Figure 5.9 shows the frequency response for various voltage amplitudes.
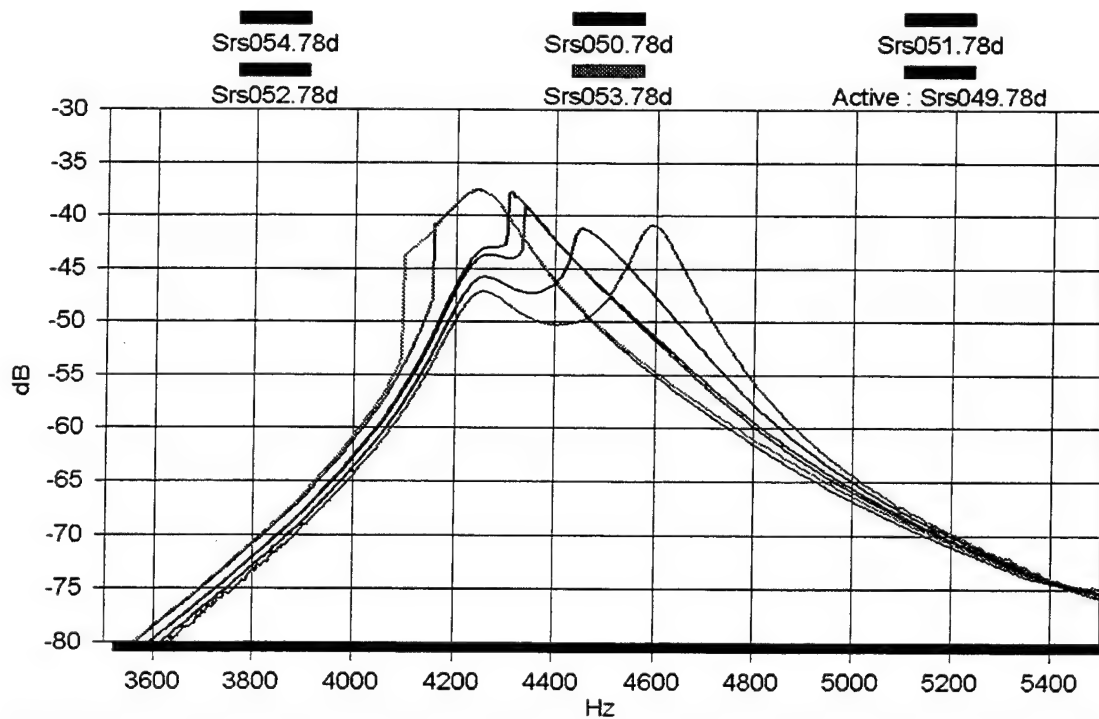
Figure 5.9 Dynamic pressure transducer output to drive voltage ratio for plunger position at 5mm. Pm = 3.45 bar. Drive voltages are: 1 Vrms (series 049), 4 Vrms, 8 Vrms and 14 Vrms (series 053 & 054). The last two drive voltages are swept up and down in frequency illustrating open hysteresis loops.

Since the acoustic impedance of the driver and resonator tube must be matched for optimum performance, this matching process may cause the resonant frequency of the combined system to be slightly different than either of the two independent resonant frequencies.

The measurements made for matching the resonance frequency are swept sine transfer functions of the pressure response relative to the drive voltages, performed at various amplitudes. Very many measurements had been made for different plunger positions. The highest peak in the pressure transfer function is obtained with a plunger position of 5 mm at a resonant

frequency of 4.300 kHz. It was clear at this point in time, that this driver was not able to produce sufficient acoustic power.

D. TEST RESONATOR MEASUREMENTS REPEATED

Unsatisfied with these measurements, additional measurements are made to be sure that our preliminary measurements have been taken properly and to collect some different data. In repeated measurements a much smaller increment is used for the plunger positions. After much more measurement and data analysis, it is determined the most representative configuration for the system is a plunger position of 5 mm with a mean pressure of 150 psia at 14 V rms drive amplitude. This configuration is most representative of the acoustic load presented by the actual refrigerating resonator when it is completed. The results from analysis are shown in the following graphs.

Pressure amplitude is set at 150 psia (10 bar). Since the test resonator does not have a thermoacoustic stack in it, it generates the same acoustic load impedance at a mean pressure of 10 bar, which the refrigerator resonator would generate at a mean pressure of 15 bar. This factoid is based solely on DSTAR calculations. Thus, a mean pressure of 10 bar is chosen for the test resonator.

Figure 5.10 shows good resonance matching at the highest drive amplitude, and the maximum response ratio of approximately –25 dB at that drive, which corresponds to an acoustic pressure of roughly 3.6 psi pk. (See

conversion equation 5.1 below.) So the qualitative performance is good, but the quantitative acoustic amplitude is rather low.
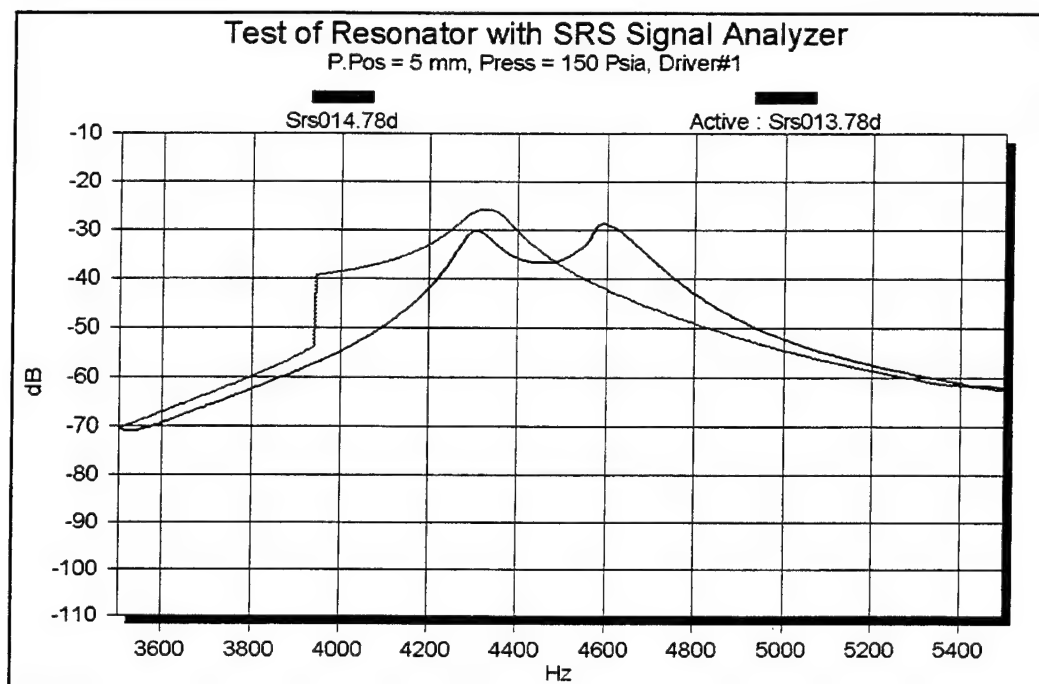
Figure 5.10. Frequency response of Driver SN-01 at 1 and 14 V-rms drive voltage

In order to better understand the characteristics of the driver and its limitations, test resonator measurements were next taken over a wide range of mean gas pressures. After the signal analyzer sweeps the system, the data is recorded. With the following equation, the acoustic pressure amplitude Po is calculated.

$$Po = 10^{(dB/20)} * V_d * \sqrt{2} /(\Pr eAmpGain * Sensitivity) \quad \text{(Eq. 5.1)}$$

where $V_d = 14$ Vrms.

The test resonator length and frequency was fixed and the mean gas pressure was varied from 0.5 bar to 15 bar. Frequency sweeps of the drive signal were performed at each pressure at maximum drive voltage and the

54

data was extracted and reduced from all of the peaks at the different mean pressures.

Vm/Vd	Pm	Po	Po/Pm	Zd	Vol Vel	Displ (pk)	Power
dB	psia	psi	%	Dyn-s/cm^5	cm^3/s	um	W
-22.71	225	4.611	2.05	41972	7.58	9.22	0.1204
-23	200	4.460	2.23	35146	8.75	10.65	0.1345
-23.95	175	3.998	2.28	28772	9.58	11.67	0.1320
-24.8	150	3.625	2.42	22807	10.96	13.34	0.1370
-26.03	125	3.146	2.52	17354	12.50	15.22	0.1356
-27.68	100	2.602	2.60	12410	14.46	17.60	0.1297
-30.49	75	1.883	2.51	8056	16.12	19.62	0.1046
-34.83	50	1.142	2.28	4379	17.99	21.90	0.0708
-38.82	35	0.722	2.06	2559	19.44	23.68	0.0484
-42.64	25	0.465	1.86	1543	20.78	25.30	0.0333
-48.46	15	0.238	1.59	715	22.95	27.94	0.0188
-52.95	10	0.142	1.42	388.0	25.21	30.69	0.0123
-57.15	7	0.087	1.25	226.5	26.63	32.42	0.0080

Table 5.1. Analysis of driver #1 using both the SRS signal analyzer and DSTAR

The first column of the table is the microphone voltage divided by the driver voltage, Vm/Vd, which is obtained from the signal analyzer curves at their peaks. The second column is the mean gas pressure of the system. The third column of the table is the acoustic pressure amplitude measured in the test resonator at the driver location in peak units, and is calculated with (eq.5.1.). The acoustic driving point impedance, Z_d of the system is calculated using DSTAR. Volume velocity is calculated in peak units with the following equation;

$$U_o = P_o/Z_d ,$$

or with units conversions to cgs,

$$VolVel = 10^6 * Po/(14.502 * Zd).$$ (eq. 5.2)

Displacement is calculated by the following equations:

$$Xo = U_o/(\omega A_p) \text{ or}$$

$$Disp = VolVel/(6.283 * PistonArea * f)$$ (eq. 5.3)

The highest acoustic amplitude that was obtained from Driver SN-01 was a pressure ratio of $p_o/p_m = 2.2\%$ at $p_m = 15$ bar. (Po is expressed in peak units.) Even this rather low number overestimates the performance because the acoustic load impedance is too high at this mean pressure. A refrigerator pressure amplitude of $p_o/p_m = 5\%$ at $p_m = 15$ bar was desired, so the measured acoustic driver performance of 3.63 psi at 10 bar must be compared to the desired operating pressure of 15 bar. This is a dynamic to mean pressure ratio of 1.61%. This value is a factor 3.1 lower than the desired 5% pressure amplitude, and thus represents an acoustic power level that is low by a factor $(3.1)^2 = 9.6$.

It was initially believed that the driver performance was limited both by the force of the PZT disk and stroke limitations of the stainless steel diaphragm. Subsequent confusion based on those assumptions caused us to re-take a large amount data over a very large range of mean gas pressures and analyze the data carefully. This analysis shown below in Figs. 5.11-13, incorporates the acoustic load impedance, Z (p_m), that DSTAR predicts.

After the calculations for table 5.1 are made, a graph for response pressure amplitudes versus mean gas pressure is constructed showing the actual acoustic pressure and force, which is created by the PZT disk.

This graph, shown in Fig. 5.11, also shows us a relation between force and acoustic impedance. By varying the mean pressure, different acoustic impedances will result, and the driver's pressure response to the varying resonator impedances is plotted.

The force delivered by the piezoceramic disk is directly proportional to the Po that we measured.

Figs. 5.12 and 5.13 shows conclusively that very large volume displacements are being achieved at low mean pressures, relative to the values at p_m = 150-225 psia. Thus diaphragm volume displacement is not a limiting factor at the acoustic load impedance range of interest. This is an important result. It means that we need to obtain more force from the PZT component. It also means that the design of Driver SN-02 was a mistake. See more on this in the next chapter.
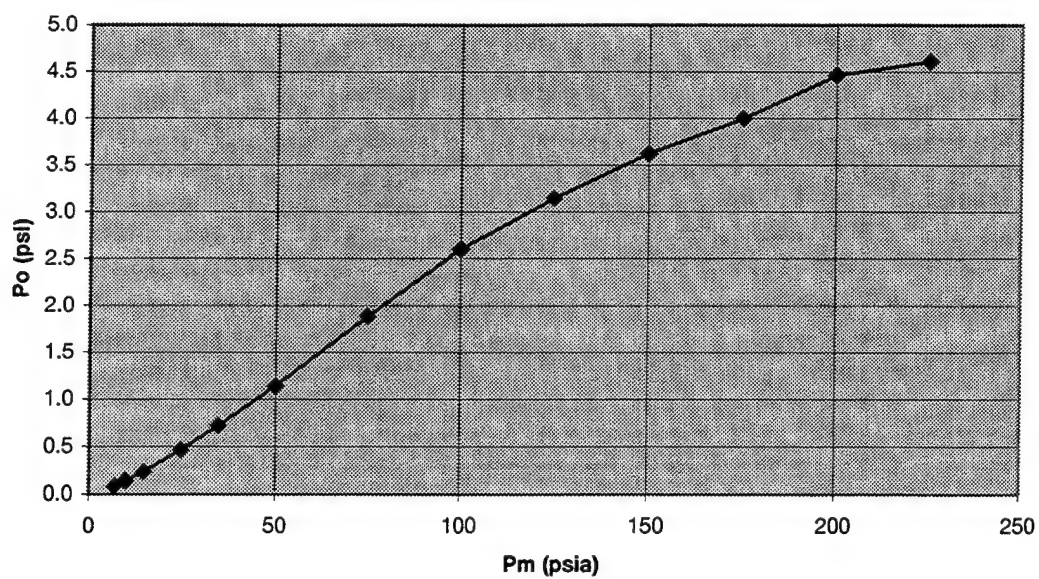
Figure. 5.11. Peak dynamic pressure vs. mean pressure
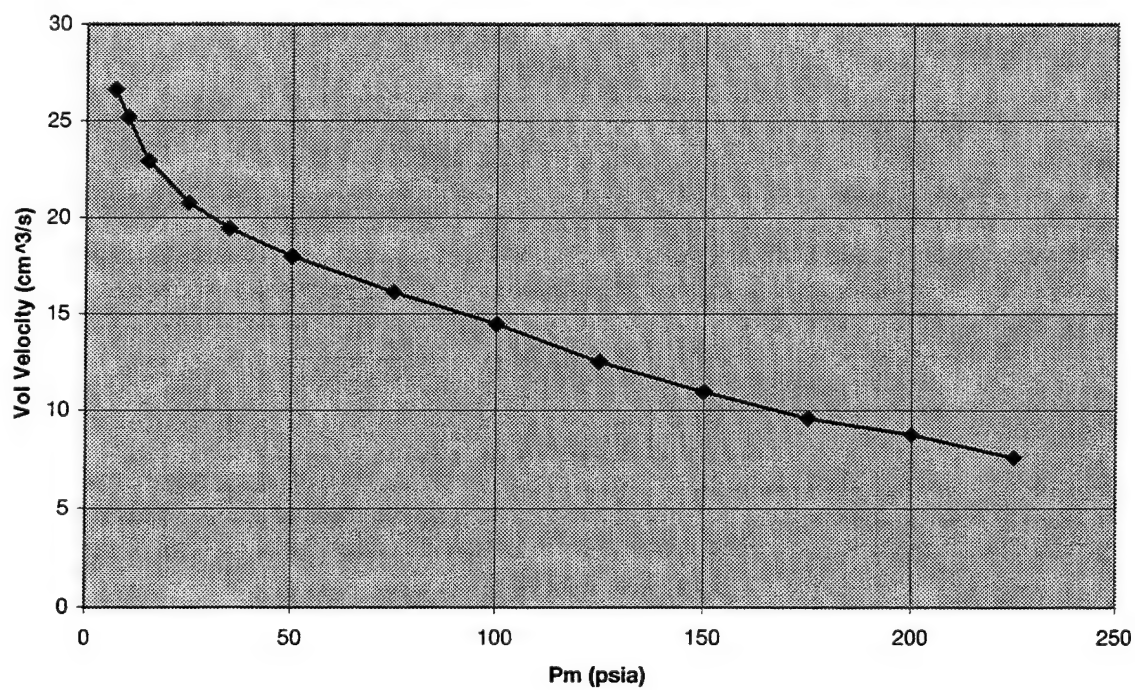
Figure 5.12. Volume velocity versus driving pressure for the single disk driver
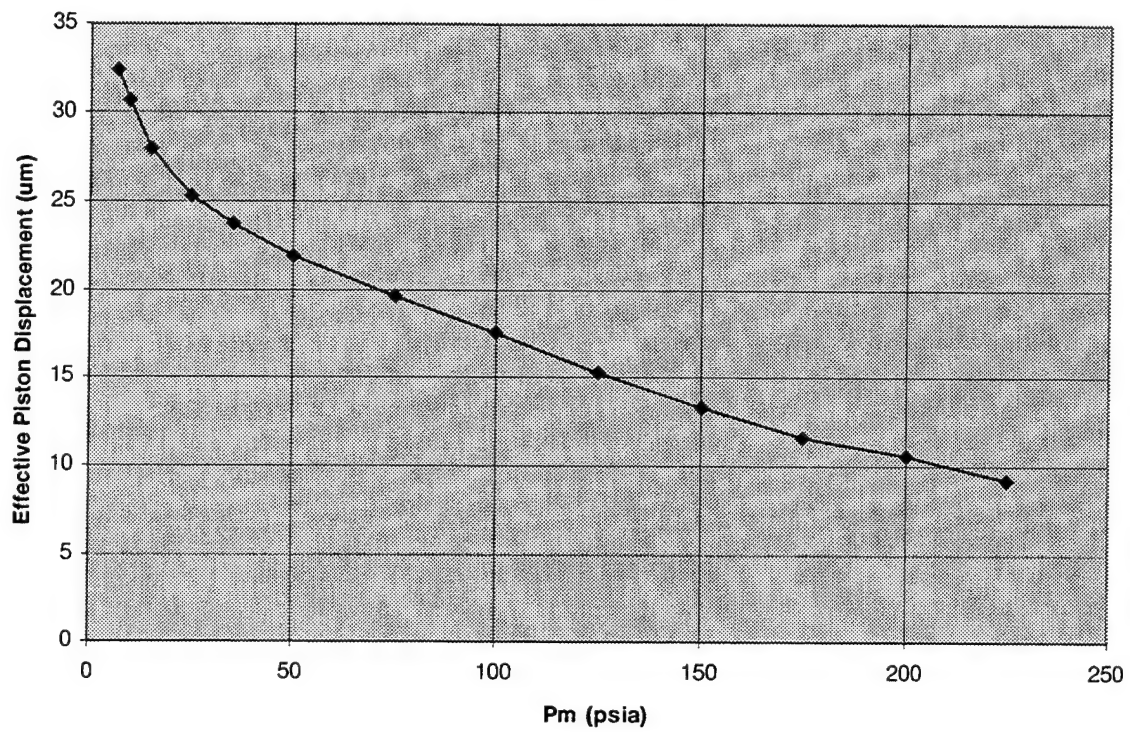
Figure. 5.13. Effective diaphragm displacement vs. mean pressure

THIS PAGE INTENTIONALLY LEFT BLANK

VI. DRIVER WITH TWO PIEZO DISKS (SN-02)

This driver was designed and constructed after SN-01, but before the data shown in Figs. 5-9 were taken. At the time it was designed, it was believed that both the diaphragm volume displacement and the force of the PZT disk were limiting factors. Thus two PZT disks were used to increase the force and a 20% larger diaphragm diameter was used. The larger diaphragm has larger area, as well as more linear stroke.

A. CONSTRUCTION

The second driver, similar to the single disk driver, has two main parts, the piezoelectric driver unit and the sealed pressure vessel unit. The latter houses the piezoelectric disks, flexible stainless steel diaphragm and the microphone. The only differences between the two drivers are that the second driver has two piezoelectric disks, and the diameter of second driver's steel diaphragm is larger than the single disk driver's steel diaphragm.

When this driver was being constructed, it was believed that both the maximum force of the single piezoelectric disk and the maximum volume displacement of the steel diaphragm was insufficient. Accordingly, the diameter of the steel disk was increased by 21%. The poor performance of the second driver perhaps shows that a larger diameter stainless steel diaphragm is not advisable for this driver.

In the driver with two disks, two piezoelectric disks are coupled together to double the amount of force delivered to the steel diaphragm. The

61

process of coupling two disks is very critical. Every disk has two power leads, positive and negative. During assembly, the correct polarity must be observed when soldering the power leads together in parallel.

Also, the two disks must face the same direction. If the disks do not face the same direction, they will be 180 degree out of phase. In this case, the two disks will vibrate in opposite directions. As a result, the magnitude of the volume displacement will be relatively small as compared to the single driver's volume displacement amplitude.

B. TESTS RESULTS FOR THE SECOND DRIVER

After the second driver had been constructed, the next step is to test the system and assess the performance of the driver. The same measurements are made for the second driver as for the first driver.

During these measurements, some difficulties have been observed. One of these difficulties is the driving voltage limitation. Since a driving voltage up to 15 V-rms is supplied to the first driver, a driving voltage of up to 10 V-rms only could be supplied to the second driver. A driving voltage that exceeds a 10 V-rms voltage breaks the solder connection of disk's power leads. Also, a voltage amplitude higher than 10 V-rms causes the epoxy joint of the two disks with the stainless steel disk to break.

The wire connection and epoxy joint problems resulting from a drive voltage higher than 10 V-rms could be the result of a 180 degree phase difference between the two disks' connection. In this circumstance, the

volume displacement at the center of disks will be small, and will be in its maximum value at the edges of the disk.

1. Displacement Measurements

The first measurement performed on the second driver is the measurement of volume velocity. For this measurement, a laser vibrometer and a sound level meter are used.

Displacement Chart For Second Driver with Laser Vibrometer
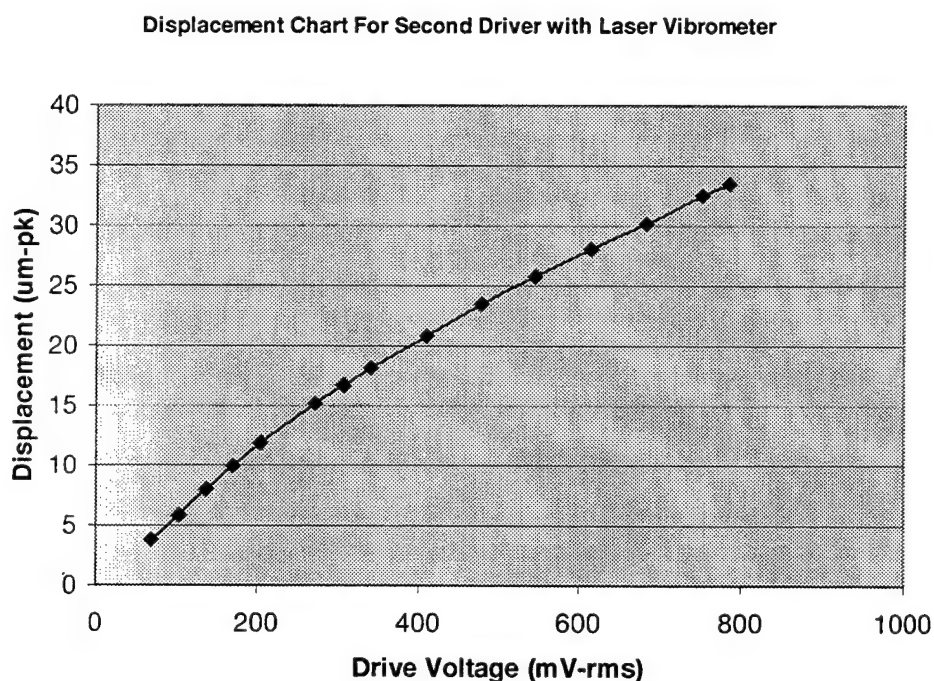
Figure 6.1. Displacement Measurement with Laser Vibrometer

The displacement chart shows that the displacement for the second driver is higher than the first driver's displacement. This displacement is measured using a laser vibrometer. As seen from the figure, the displacement is roughly proportional to the driver's input voltage.

2. Test Resonator Measurements

As previously explained, these measurements are swept sine transfer functions of microphone pressure response inside the resonator relative to the

Figure 6.2. Dynamic pressure transducer output to drive voltage ratio. Drive voltages are: 1 Vrms (series 011), 8 Vrms (series 013), and 10 Vrms (series 015). All drive voltages are swept down in frequency

drive voltage at various static pressures. Several measurements are taken at different plunger positions, various static pressures and drive voltages. The highest peak in the pressure functions is found at the 6 mm plunger position at a 4.11 kHz resonant frequency.

SRS011 has been driving with 1 V rms voltage while SRS013 had been driving with 8 V-rms and SRS015 had been driven with 10 V-rms voltages.

The performance of the Driver SN-02 was very poor in several respects. First, problems were encountered with breakage of the internal electrical

power leads to the PZT disks and breakage of the adhesive joints between the PZT disks and the aluminum push rods. Lastly, the amount of acoustic pressure and power delivered to the test resonator was very poor. The highest levels were about a factor of 2.6 lower than those of Driver SN-01.

One possible explanation for the poor performance is that the two PZT disks were mounted and wired with incorrect polarity. This possibility was checked by visual inspection and correct polarity was confirmed. There are clear markings on the disks. So unless one disk was manufactured incorrectly, this is not a good explanation. No other reasonable explanations were found.

THIS PAGE INTENTIONALLY LEFT BLANK

VII. SCHEMES TO IMPROVE DRIVER PERFORMANCE

A. THIRD DRIVER (SN-03)

The results had been discussed in Chapter V for SN-01 suggest that the original diaphragm design is quite good, so Driver SN-03 has the exact same diaphragm as Driver SN-01. Since more drive force is required and no satisfactory explanation for the problems of Driver SN-02 were found, it was decided to try to double the force with two PZT disks again, but with the original diaphragm dimensions.

Since the driver with one disk (SN-01) and driver with two disks and larger steel diaphragm (SN-02) could not produce the expected dynamic pressure ratio (Po/Pm) a third driver had been designed and constructed. This third driver (SN-03) contains two PZT disks. The only design difference between third driver and second driver is in the stainless steel diaphragm. The third driver's steel diaphragm is the same as the SN-01 diaphragm and is smaller than the second driver's diaphragm.

As explained in Chapter VI, the second driver could only be driven up to 10 Vrms without mechanical damage, whereas the third driver could be driven up to 14 Vrms. With this driver the difficulties discussed in Chapter VI had not been observed.

The driver and test resonator system was swept with the SRS signal analyzer and driver SN-03. The test resonator was pressurized to 150 psia and various plunger positions and voltage amplitudes were measured.

Plunger positions varied from 10 mm to 2 mm with 0.5 mm decrement. The highest dynamic pressure ratio had been observed at 6.5 mm plunger position.

Test of Resonator with SRS785 Signal Analyzer
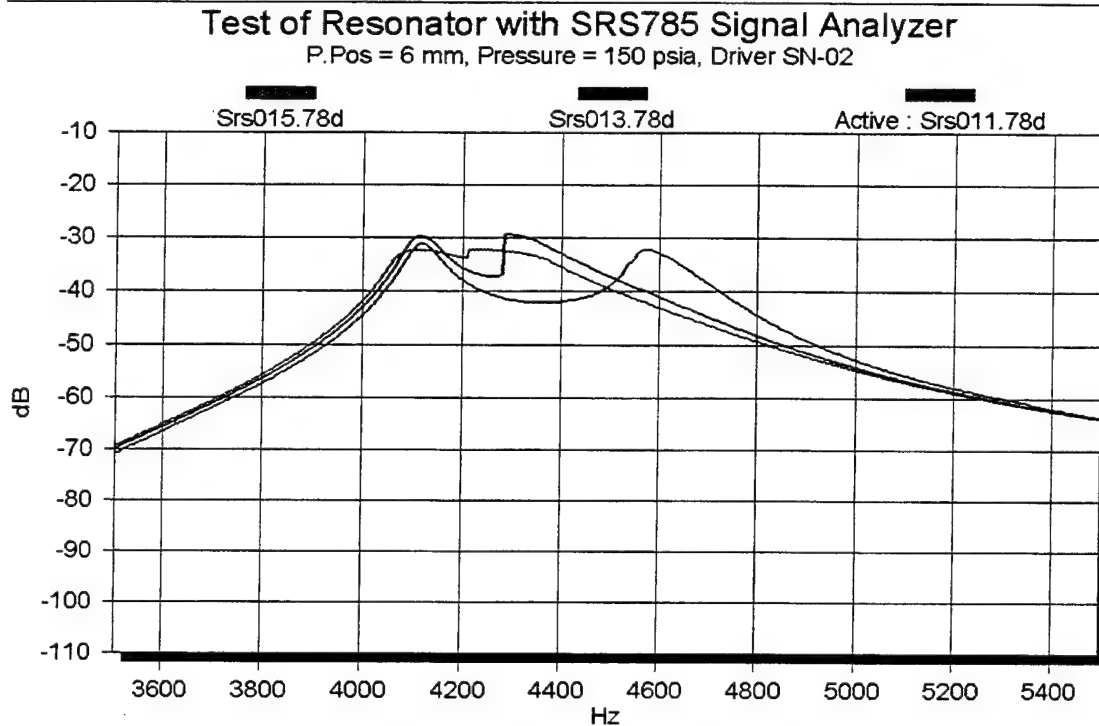### P.Pos = 6.5 mm, Press = 150 psia, Driver SN-03
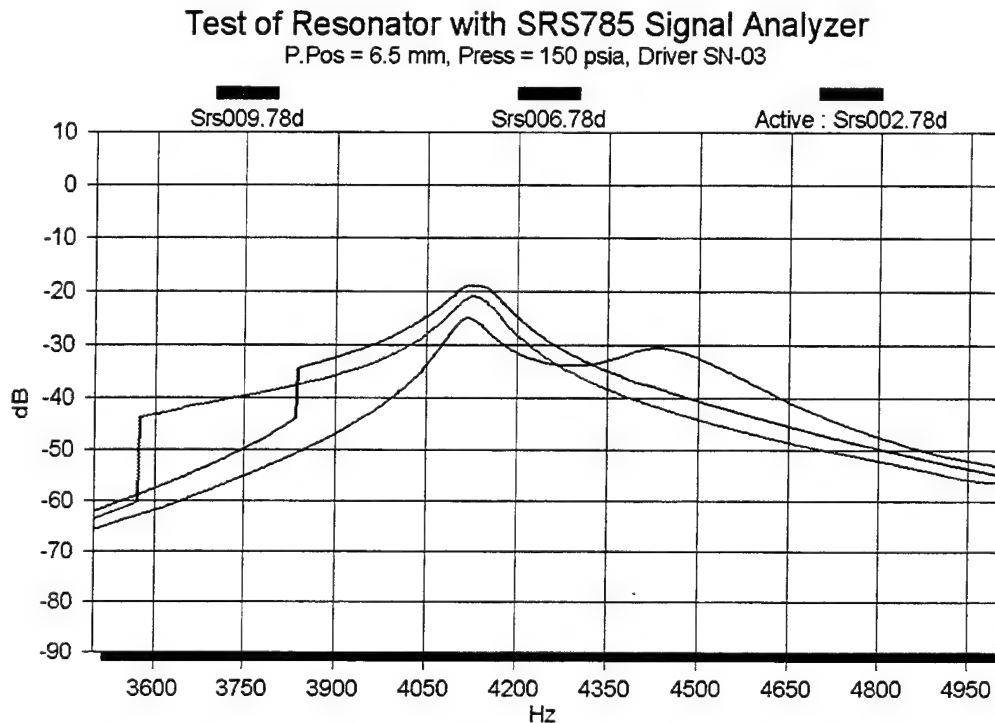
Figure 7.1. Dynamic pressure transducer output to drive voltage ratio. Drive voltages are: 1 Vrms (series 002), 8 Vrms (series 006) and 14 Vrms (series 009).

As seen from the figure above, 4120 Hz resonant frequency had been observed for the test resonator at this plunger position. The three curves in Fig. 7.1 represent drive voltages of 1 V rms, 8 V rms, and 14 V rms.

Figure 7.1 shows a higher dynamic pressure to drive voltage ratio at 8 V rms than at 1 V rms because the driver's nonlinear mechanical resonance has shifted from 4430 Hz at the lower amplitude to roughly 4120 Hz at the higher amplitude. The lower frequency best matches the test resonator's frequency and produces higher relative dynamic pressures. However, when driven at 14 V rms, the dynamic pressure to drive voltage decreases

68

somewhat. This effect is most likely the result of intrinsic saturation of the piezoceramic material.

After the highest dynamic pressure ratio had been observed at the 6.5 mm plunger position at 150 psia pressure, the system was then driven over a wide range of many drive voltages. The system was measured at 9 different drive voltages from 0.5 Vrms to 14 Vrms.

The Po values for 6.5 mm plunger position at 150 psia pressure amplitudes at various drive voltages are shown in the Table 7.1. These values show that this Driver SN-03 provides a better response when compare to the SN-02 which its values is given in Chapter VI.

Test of Resonator with SRS785 Signal Analyzer			
Pressure		150 psia	
Microphone Sensitivity		26.8 mV/psi	
dB	Drive Voltage(Vrms)	Frequency(Hz)	Po (psi)
-25.25	0.5	4116	0.144
-25.07	1	4114	0.294
-22.57	2	4116	0.785
-20.85	4	4105	1.914
-19.23	6	4123	3.459
-18.98	8	4122	4.747
-19.33	10	4131	5.699
-20.22	12	4128	6.173
-21.04	14	4131	6.553

Table 7.1. Po values for various drive voltages.

As seen from the table above, Po increases with drive voltage. The acoustic amplitudes shown in Fig. 7.2 are higher than those obtained with Driver SN-01, by a factor of 1.8, so the force is not exactly a factor of two

higher, but reasonably close. Furthermore, the acoustic amplitudes are now within the range necessary to produce useful thermoacoustic refrigeration cooling power, although not quite as high as originally planned. As can be seen in Fig. 7.2, the response versus drive voltage curve is not perfectly linear with a reduction in response occurring at higher amplitudes. Again, this is likely a characteristic of the piezoceramic although it could represent some further frequency shifting of the driver resonant frequency.
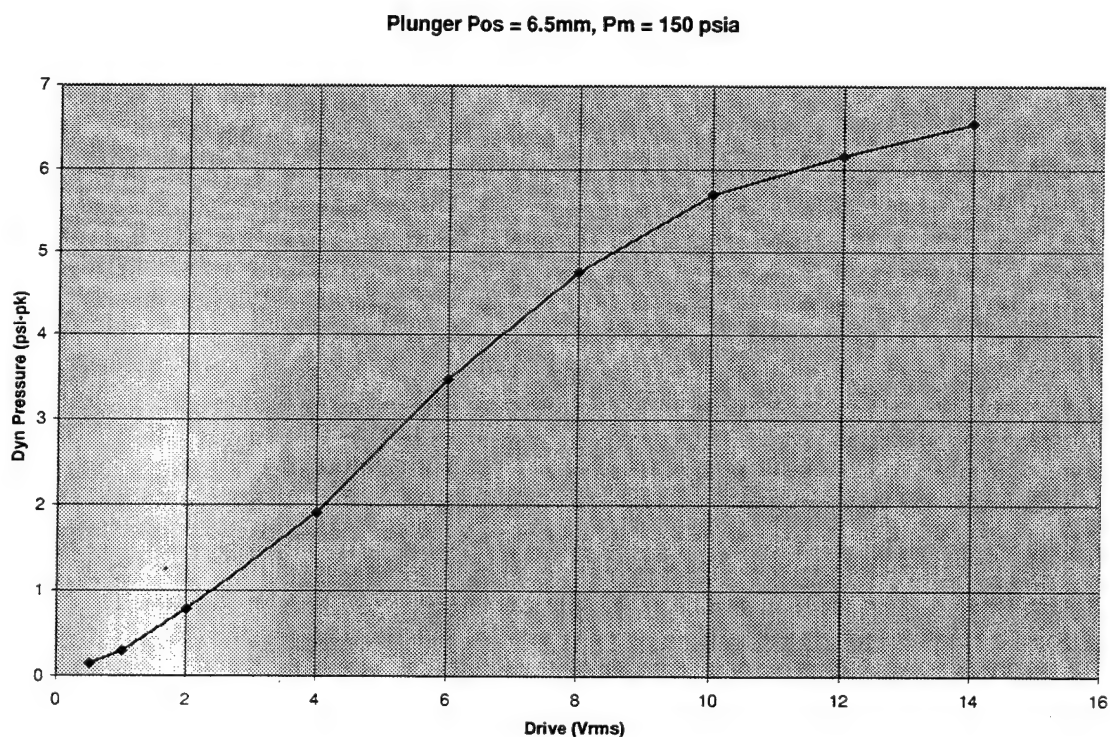
Plunger Pos = 6.5mm, Pm = 150 psia

Figure. 7.2. Acoustic pressure generated vs. mean gas pressure.

Also, the operational behavior of Driver SN-03 has been without incident. No breakage or failure problems have been encountered. We expect

that Driver SN-03 will be used for actual refrigeration tests, when the refrigerator resonator is ready.

B. MASS LOADING OF OUTER EDGE OF PZT CERAMIC DISK

Another possible scheme to extract more acoustic power from the standard PZT bimorph disk consists of attaching several tiny lead masses to the outer edge of the disk adhesively.

The masses were pieces sliced from 1.6 mm diameter lead wire. Approximately 0.16 gm of mass was added to a bare PZT disk with a bare mass of 1.17 gm. Some preliminary data was taken with a laser vibrometer.

The vibrometer velocity data was taken of a freely suspended disk under conditions of nearly zero acoustic loading. The limited range of the laser vibrometer instrument prevents data from being taken at the higher amplitudes. Initial results show some increase in disk displacement with less than 5% drop in resonant frequency. This result is promising and we are planning to repeat the test with more care.

While the goal is to increase the force of the PZT disk, the above measurement is considerably easier to do. An increase in maximum disk displacement under no load, should translate into more force for a given finite acoustic load impedance.

We also planned to construct another pressurized driver using a single weighted disk. This will take some time since more parts need to be

machined and another difficult electrical feedthrough plate must be fabricated. This driver will not be a part of this thesis.

VIII. REFRIGERATOR RESONATOR

Before designing a mini thermoacoustic refrigerator, its performance expectations must be defined. The mini TAR will be designed according to these performance expectations. All other properties of the mini TAR, such as the parameters of the driver, the length of tube or the pressure of the gas in the tube, are all related to the definitions of these performance expectations. With the aid of computer programs, it is possible to calculate the outputs and define thermoacoustic requirements before building hardware.

The Design Simulation for Thermoacoustic Research (DSTAR) computer modeling software can be used to determine the mini TAR's thermoacoustic requirements. DSTAR is a Windows™-compliant graphical based program that provides a flexible and powerful tool for the design and analysis of thermoacoustic heat engines.

All the details about design criteria, the DSTAR model and basic hardware design is explained by Livvarcin. The following information has been taken from Livvarcin. [ref 9]

A. BASIC DESIGN CRITERIA

1. Thermoacoustic Requirements For The Mini Tar

Rockwell, the corporate sponsor of the mini TAR development project, defined the original performance expectations for the mini TAR. Rockwell envisioned a mini TAR that would operate around 10 kHz, with 1 W cooling power between 60°C and 90°C, and a 1-inch total length. But due to the difficulties encountered, (i.e., finding a driver with 10 kHz frequency and designing very small components) the performance expectations were subsequently modified. The project's ultimate goal is to design an acoustic mini TAR with 1 W cooling power (between the temperatures mentioned above) that can operate at around 4 kHz. The length of the prototype is also increased from its original length of 1 inch to roughly 2.5 inches.

These specifications for the design of the mini TAR are dependent upon other variables such as the type and the pressure of the gas in the tube, the length of the tube, the diameter of the driver and the Po/Pm ratio. The mini TAR model in this thesis assumed constraints of 15 bars of gas pressure in the tube (a He-Kr mixture with 5% Kr atomic), 4 kHz operating frequency, a modified quarter wavelength resonator vessel and a 5% dynamic pressure ratio, Po/Pm, (or the ratio between the peak dynamic pressure and the pressure of the gas in the tube).

2. Rational for Assumed Constraints

The dynamic pressure ratio is the ratio between the peak dynamic pressure and the pressure of the gas in the tube, and can be calculated using the following equation:

$$\text{Dynamic pressure ratio} = \frac{P_0}{P_m} \tag{8.4}$$

In this project, the numerical design model used in DSTAR assumes a dynamic pressure ratio around 5 %.

The Po/Pm value of 5% is an ad-hoc constraint based on experience and results with previous thermoacoustic refrigerators. This pressure amplitude value has been achieved previously here at NPS with other refrigerators,[Lesperance thesis] but is at the upper end of the scale. A large amplitude and the resulting high cooling power density in the stack are beneficial in competing against the negative effects of thermal conduction in the stack region. In tiny refrigerators the temperature gradients are necessarily quite large and the problem of thermal conduction heat transfer becomes much worse. Of course, even higher-pressure amplitudes might be extraordinarily difficult to achieve.

One other parameter closely related to the dynamic pressure ratio is the pressure of the gas in the tube. The DSTAR model assumes that the mean pressure of the gas should be 15 bar. Below 15 bar, the total acoustic power will decrease, causing a corresponding drop in the TAR cooling power. Also, lower pressures mean the acoustic penetration depth will increase.

Increases in penetration depth increase the acoustic dissipation in the resonator. Mean pressures much higher than 15 bar will make the acoustic penetration depth too small which would exceed our ability to fabricate the requisite thermoacoustic stack. The fine internal structure of the thermoacoustic stack must match the size of the penetration depth.

The operating frequency constraint of 4 kHz is determined by the fundamental mechanical resonance of the commercially available piezoelectric disks.

B. DESIGN WITH DSTAR

The DSTAR software allows the analysis of the thermoacoustic-wave and energy-transfer equations from the beginning of a thermoacoustic heat engine to the end, on a component-by-component basis. This approach allows the user to change the configuration and parameters of the individual components of the heat engine "on the fly" with DSTAR recalculating the effect of the changes on the overall solution of the heat engine. (Curtis, 2000)

Some parameters such as acoustic amplitude and gas pressure can be varied at-will in the experimental phase of the project, in order to explore the performance characteristics of the prototype. Small improvements in efficiency can be obtained by the combined adjustment of these and other parameters. The resulting experimental optimum is often slightly different than the predictions produced by the linear DSTAR models.

Other parameters, or combinations of parameters, are quite sensitive to variations or errors, and must be determined precisely. One such combination is the resonator length and the drive frequency. The overall resonator length is considerably less than a quarter of a wavelength because of the shaped diameter changes of the resonator. The shaped tubing reduces acoustic dissipation greatly and improves efficiency, while making the resonator more compact. For 4 kHz, a quarter wavelength is:

$$\frac{\lambda}{4} = \frac{c}{4*f} = \frac{727 \, m/s}{4*4000 \, Hz} = 45.44 \, mm$$

The piezoelectric flexural disk has a its own resonance, with a rather narrow operating frequency range. Changes in the resonant frequency of the disk demand that the length of the resonator should be changed correspondingly. (Another experimental option is to vary the concentration of the Kr in the HeKr gas mixture thereby altering the sound speed.) These facts necessitate understanding and testing the operation of the disk and driver prior to completing the resonator design. Changing the resonator design to match shifts in the operating frequency of the driver can be accomplished easily with the aid of DSTAR.

With the final design shown in Fig. 8.1 below, the DSTAR solution gives a result of 2.35 W of cooling power over a 30° C temperature span while utilizing 1.3 W of acoustic power delivered by the driver. These numbers

yield an acoustic to thermal coefficient-of-performance or COP of 1.81. (The COP defined here is the cooling power to acoustic power ratio.)

The DSTAR model does not include the thermal conduction of the stainless steel tube we intend to use to hold the stack. This conduction is estimated to be 0.675 W, so that the net cooling power is now 1.675 W for a net COP of 1.3.

C. DESIGN OF THE MINI TAR

The mini TAR consists of two main parts. The first one is the driver and second one is the resonator vessel. The figure below shows the whole device with both major components. The driver shown is the 2nd constructed driver with two piezoelectric disks and larger steel diaphragm, which will not be used because of its poor performance. The actual driver will be very similar except for the diaphragm diameter.

There is a moderate amount of design detail relating to the resonator vessel shown in Fig. 8.1, however the discussion of these details is beyond the scope of the thesis.
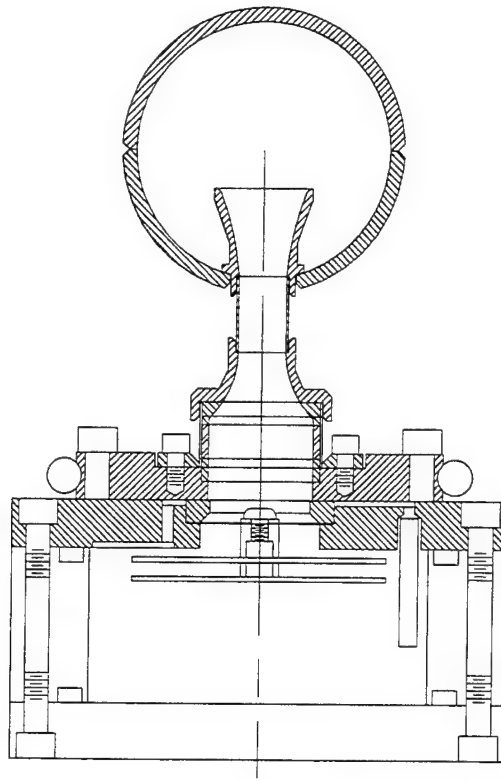
Figure 8.1. The Steel resonator shown attached to a double disk driver

THIS PAGE INTENTIONALLY LEFT BLANK

IX. CONCLUSIONS

A. THERMOACOUSTIC REFRIGERATION

Thermoacoustic refrigeration is a new concept in refrigeration technology. Although thermoacoustic experiments have been performed for the last 17 years, actual usage of thermoacoustic refrigerators (TAR) in technology has not been applied.

There are some reasons why TARs are impractical. First, they are not as efficient as traditional vapor-compression refrigerators in terms of energy consumption. Although there have been some experimental improvements, the TAR's cooling efficiency is still below acceptable limits, since the efficiency of traditional refrigeration continues to improve. Secondly, when compared with traditional refrigeration systems TARs are not cost effective. And finally, since the technology is new, research and development is required to satisfy the performance requirements defined by Rockwell.

Nevertheless, there may be some exceptions in which the benefits of using a TAR surpass those of other systems. TAR technology may be superior to either traditional vapor-compression refrigeration or Stirling refrigeration in the context of miniature devices spanning modest temperature differences. Miniaturization is likely to be too difficult for vapor-compression or Stirling technologies.

Also, TARs may have some advantages in satellites or aircraft. There are also specific contexts in which the TAR is the only feasible refrigeration

option, wherein other systems would be incompatible. Hot environments preclude the use of current thermoelectric devices. Also, a TAR device should have higher cooling efficiency than current generation thermoelectric devices.

Internationally, scientists are making efforts to improve TARs. The experimental results show promising potential for the future of this new technology.

B. THE MINI TAR

The mini TAR is one of the newest practical applications of the TARs. This name has been given due to its small size. All thermoacoustic laws apply to mini TARs as well as to any other TAR. In the near future it may be possible to see mini TARs installed on high-tech military instruments. The application of mini TAR in civilian technology may take longer because of the high cost of this new technology or its unfamiliarity.

C. THIS THESIS AND FURTHER EFFORTS

The goal of this thesis was to design, develop and test a mini TAR driver. The design of the new TAR, while similar to the previous designs, is more complex due to its smaller size. The design of the driver is new.

Contrary to the previous TAR models, the mini TAR has unique small parts, which are not easily acquired. Almost all of the parts are designed and manufactured by Naval Postgraduate School personnel in Monterey, California. Even the piezoceramic disk, which was originally manufactured

by Motorola, has been modified significantly so it could be used in the driver unit.

The mini TAR has two main units, the driver and the resonator. Although a test resonator was used for measurements, this thesis focused on the driver performance. The objective was to fully characterize the drivers and to produce a drive unit capable of delivering sufficient acoustic power to the eventual TAR resonator.

Also in terms of performance, the resonator is equally as important as the driver. The properties of the stack and the gas inside the resonator tube are crucial parameters, as are those of the resonator. Further research efforts had been done to obtain the optimal resonator length and properties.

The measurements with Driver SN-01 show that the driver performed qualitatively as expected, but with less acoustic amplitude than that required for the refrigerator. The highest acoustic amplitude that was obtained from Driver SN-01 was a pressure ratio $p_o / p_m = 2.4\%$ peak at $p_m = 10$ bar, while a refrigerator pressure amplitude $p_o / p_m = 5\%$ at 15 bar was desired. For reasons explained in Chap. 5, this implies the driver performance is roughly a factor of 10 too low in acoustic power.

The performance of the Driver SN-02 was very poor in several respects. First, problems were encountered with breakage of the internal electrical power leads to the PZT disks and breakage of the adhesive joints between the PZT disks and the aluminum push rods. And lastly, the amount of acoustic

83

pressure and power delivered to the test resonator was very poor. The highest levels were about a factor of 2.6 lower than those of Driver SN-01.

The acoustic amplitudes of Driver SN-03 are higher than those obtained with Driver SN-01 by a factor of 1.8, which implies an acoustic power increase of 3.25. Furthermore, these acoustic amplitudes are within the range necessary to produce useful thermoacoustic refrigeration cooling power.

We expect that Driver SN-03 will be used for actual refrigeration tests, when the refrigerator resonator is ready. The bulk of effort until now has been involved in driver development. Driver SN-03 should be adequate for refrigeration tests with an acoustic power delivery of about 0.5 W.

LIST OF REFERENCES

1. Swift, G.W., "Thermoacoustic Engines and Refrigerators", Physics Today, pp. 22-28, July 1995.

2. Purdy, E.W., "Development of a Graphical Numerical Simulation for Thermoacoustic Research", December 1998.

3. Wheatley, J.C., Swift, G.W., and Migliori, A., "The Natural Heat Engine", Los Alamos Science, number 14, pp. 2-29, Fall 1996.

4. Moran, M.J., Shapiro, H.N., Fundamentals of Engineering Thermodynamics, John Wiley and Sons, 1988.

5. Swift, G.W., "Thermoacoustic Engines", Journal of the Acoustical Society of America, v.84, p. 1145-1179, 1988.

6. Wong, K., "Solving Ordinary Differential Equations with Runge-Kutta Methods", June 1996, [www.geog.ubc,ca/numeric/labs/lab4/lab4/lab4.html].

7. Kreyszig, E, Advanced Engineering Mathematics, 6th ed, John Wiley and Sons, 1988.

8. Allen, R.C., Avery, P., and Wallace, J.Y., "Lower/Upper Triangular (LU) Decomposition", Computational Science Textbook, Sandia Corporation, 1998, [ais.cs.sandia.gov/AiS/textbook/textbook.html].

9. Livvarcin, O., "Design and Cost-Benefit Analysis of a Mini Thermo-Acoustic Refrigerator Driver", September 2000

THIS PAGE INTENTIONALLY LEFT BLANK

INITIAL DISTRIBUTION LIST

1. Defense Technical Information Center   2
    8725 John J. Kingman Rd., STE 0944
    Ft. Belvoir, VA 22060-6218

2. Dudley Knox Library   2
    Naval Postgraduate School
    411 Dyer Rd.
    Monterey, CA 93943-5001

3. Professor T. Hofler, Code PH/HF   4
    Naval Postgraduate School
    Monterey, CA 93943-5001

4. Professor R. Harkins, Code PH/HF
    Naval Postgraduate School
    Monterey, CA 93943-5001   1

5. Turkish Navy Headquartes   1
    DzKK Bakanliklar
    Ankara-Turkey

6. LTJG Seyhmus Direk   2
    Ozkan Pasaji No 11.
    Viransehir 63700 /Sanliurfa
    TURKEY

7. Deniz Harp Okulu Kutuphanesi
    Tuzla Istanbul   1